On the fundamental and practical aspects of modeling complex electrochemical kinetics and transport

Steven C. DeCaluwe[*], Peter J. Weddle[*], Huayang Zhu[*], Andrew M. Colclasure[**], Wolfgang G. Bessler[†], Gregory S. Jackson[*], and Robert J. Kee[*]

[*] *Department of Mechanical Engineering, Colorado School of Mines, Golden, CO 80401, USA*

[**] *National Renewable Energy Laboratory, Golden CO 80401, United States*

[†] *Institut für Energiesystemtechnik, Hochschule Offenburg, 77652 Offenburg, Germany*

Abstract

Numerous technologies, such as batteries and fuel cells, depend on electrochemical kinetics. In some cases, the responsible electrochemistry and charged-species transport is complex. However, to date, there are essentially no general-purpose modeling capabilities that facilitate the incorporation of thermodynamic, kinetic, and transport complexities into the simulation of electrochemical processes. A vast majority of the modeling literature uses only a few (often only one) global charge-transfer reactions, with the rates expressed using Butler–Volmer approximations. The objective of the present paper is to identify common aspects of electrochemistry, seeking a foundational basis for designing and implementing software with general applicability across a wide range of materials sets and applications. The development of new technologies should be accelerated and improved by enabling the incorporation of electrochemical complexity (e.g., multi-step, elementary charge-transfer reactions and as well as supporting ionic and electronic transport) into the analysis and interpretation of scientific results. The spirit of the approach is analogous to the role that CHEMKIN has played in homogeneous chemistry modeling, especially combustion. The CANTERA software, which already has some electrochemistry capabilities, forms the foundation for future capabilities expansion.

Keywords: Marcus theory, Butler–Volmer kinetics, CANTERA, Ion and electron transport, Faradaic and Ohmic heating, General-purpose software

Contents

1. Introduction

Electrochemistry plays a central role for technologies in energy conversion, energy storage, and material/chemical processing. Corrosion processes and their mitigation are also grounded in electrochemistry. Electrochemical systems such as batteries and fuel cells can provide primary or auxiliary power with high efficiency and low environmental impact for a range of vehicular or stationary applications. However, improved energy density, durability, and safety are neede d to enable broader deployment. Such technological advances must build on fundamental understanding of electrochemical processes over many scales. Flexible and robust computational tools can play a key supporting role in accelerating that understanding and promoting technology breakthroughs. Advances in atomistic computational modeling have enabled the identification of materials with finely tuned properties at the nanoscale [1–5], but the lack of concurrent development of modeling frameworks at the device scale impedes the translation of these materials into practical electrochemical devices and systems.

With only a few exceptions, the electrochemistry modeling literature is based on using a very few (often one per electrode) global charge-transfer reaction steps [6–9]. In reality, the heterogeneous chemistry and electrochemistry is far more complex. For example, in Li-ion batteries, the formation of solid-electrolyte-interface (SEI) films is known to involve complex chemistry and electrochemistry [3, 10, 11]. Solid-oxide fuel cells operating on hydrocarbon fuels are typically modeled with two global reforming reactions and one charge-transfer reaction. The actual chemistry is significantly more complex. Beyond these, numerous other technology examples involving electrochemistry can benefit from more complete electrochemical modeling and simulation tools. However, new software frameworks are needed to handle the necessary complexity.

The lack of general software for expressing electrochemical complexity limits the practical ability to introduce such complexity into experimental interpretation and technology development. This is not to be critical of current modeling efforts, which are certainly effective and useful. Rather, it expresses the opportunities for significant and beneficial improvements. The primary objective of the present paper is to identify the scientific needs and to explore opportunities for computational implementation. New modeling capabilities should be closely coupled with functional relationships, properties, and parameters that can be readily extracted from atomistic modeling or basic analytical measurements, rather than from empirical parameter fits that are difficult to generalize.

Fundamental and theoretical underpinnings for electrochemistry, which are generally documented in textbooks [12–15] and a vast archival literature, certainly cannot be fully explained in a few pages. Thus, the intent of the present writing is to highlight areas where new modeling frameworks can offer substantial value. Drawing from illustrative applications in batteries, fuel cells, electrolyzers, and membrane reactors, the discussion shows how development and deployment of new generalized capabilities can enable modeling of complex electrochemical processes, significantly assisting the design of new high-performance electrochemical systems and thereby accelerating the pace of technology development. While the focus of the present paper is on modeling tools and not on simulation, we present a brief discussion on how generalized modeling tools can enable adaptations necessary for varying simulation methodologies. Finally, we conclude by proposing a generalized user input file to fully describe the range of electrochemical complexity in a Li-ion battery. The file is written within the context of the CANTERA software package [87], which is an open-source suite of object-oriented software tools for calculating chemical kinetics, thermodynamics, and/or transport processes to support simulation of chemical and electrochemical processes. The example of CANTERA is meant to be generally illustrative of the breadth and depth of user inputs

required for any generalized electrochemical modeling tool.

2. Illustrative examples

Before discussing the important quantitative relationships needed for electrochemical modeling, it is useful to consider illustrative examples of electrochemical devices. The example devices presented here vary in chemical and electrochemical complexity, and demonstrate the broad applicability of the advanced electrochemical modeling concepts discussed herein. By analyzing how these example devices are modeled, overarching modeling needs and capabilities for next-generation software become evident.

2.1. Lithium-ion batteries

Lithium-ion batteries represent a widely used and rapidly changing electrochemistry technology. With only a few exceptions, the majority of the modeling literature is based on an approach developed by Newman and colleagues [12, 16, 17]. Figure 1 illustrates the central tenets of the Newman model. During discharge, an electrochemical charge-transfer reaction removes Li from the anode phase, delivering Li^+ ions into an electrolyte solvent and electrons into the anode phase. The Li^+ ions are transported within the electrolyte solvent by diffusion and migration through the separator into the cathode side of the cell. Charge transfer chemistry reacts a Li^+ from the electrolyte phase with an electron from the electrode phase (coming from an external circuit) to deliver charge-neutral Li into the cathode phase. The electrodes themselves are assumed to be composed of spherical graphite particles for the anode and spherical metal-oxides for the cathode. The Newman model is frequently referred to as a 'pseudo-2D' model: electronic and ionic charge transport (in the electrode and electrolyte phases, respectively) are modeled in the 'through-cell' direction, while charge-neutral lithium intercalates within the particles via diffusion.

Charge-transfer chemistry at the electrode-electrolyte interfaces is usually modeled using a global reaction as

$$\mathrm{Li(ed)} \rightleftharpoons \mathrm{Li^+(el)} + \mathrm{e^-(ed)}, \tag{1}$$

where Li(ed) represents a charge-neutral Li incorporated in the electrode, Li^+(el) represents a Li ion within the electrolyte, and e^-(ed) represents an electron within the electrode phase. As written, the forward direction is anodic, meaning that the reaction produces electrons. This would be the case for a battery anode during discharge

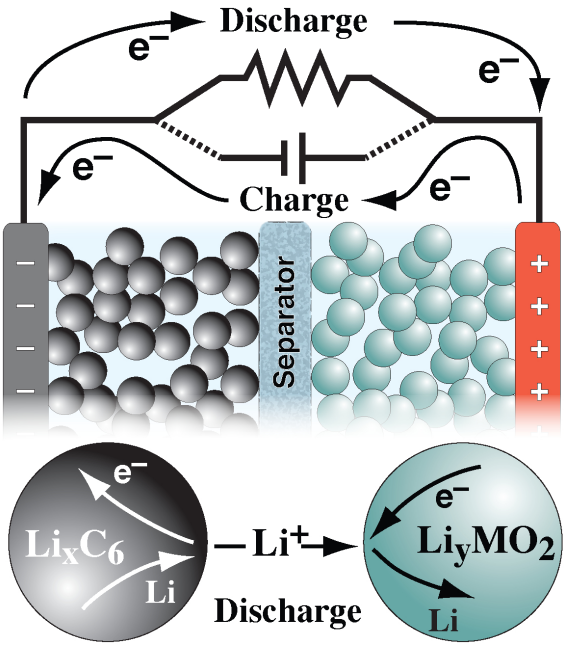

Figure 1: Illustrative aspects of a Newman Li-ion battery model.

or a battery cathode during charging. Although this reaction may be a reasonable approximation under many circumstances, it is certainly a simplification of the actual chemistry.

An alternative representation of the charge-transfer chemistry employs a two-step process, which may be expressed as [9, 18]

$$\mathrm{Li(ed)} + \mathrm{(s)} \leftrightarrows \mathrm{Li(s)} + \mathrm{V_{Li}(ed)}, \tag{2}$$

$$\mathrm{Li(s)} \leftrightarrows \mathrm{Li^+(el)} + \mathrm{e^-(ed)} + \mathrm{(s)}, \tag{3}$$

where (s) is a vacant surface site, Li(s) is the lithium on the electrode surface, and V_{Li}(ed) is a lithium vacancy within the graphite electrode lattice structure. In this representation, Reaction 3 is the charge-transfer step, whose rate depends on concentrations and electrostatic-potential differences. Reaction 2 is a heterogeneous surface reaction that depends on species concentrations, but not directly on electrostatic potentials. Even this relatively straightforward two-step process introduces electrochemical complexity that is not typically practiced in Li-ion battery models.

Although Fig. 1 illustrates the electrodes as spherical particles, and typical models represent the electrode particles as spheres, the actual electrodes are far more complex. Figure 2 illustrates a microscale reconstruction of a commercial Li_xCoO_2 cathode. The "particles" have irregular shapes and are overlapping. The carbon-based binder is seen as black in Fig. 2. The open pore space would be filled with a Li-ion-conducting solvent. Mod-

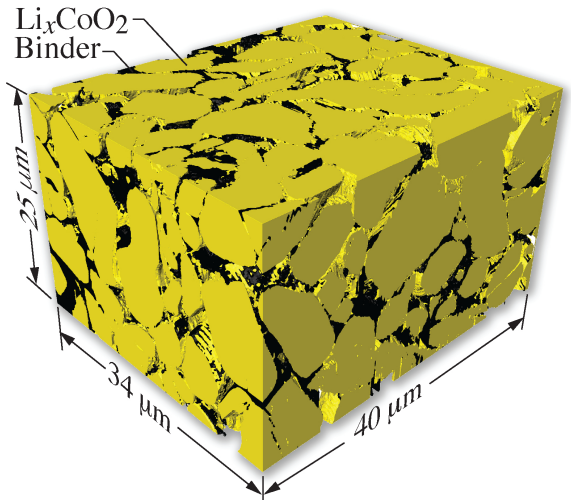

Figure 2: Three-dimensional reconstruction of a commercial Li_xCoO_2 cathode. The microscale reconstruction was created using Focused-Ion-Beam–Scanning-Electron-Microscopy (FIB-SEM). This image was produced by Prof. Scott Barnett, Northwestern University.

els that deal with electrochemistry at the electrode microscale must be concerned with geometrical complexity as well as electrochemical complexity [19].

Figure 3 illustrates a Li-ion battery based on a lithium-titanate ($Li_4Ti_5O_{12}$, LTO) anode and a lithium-iron-phosphate ($LiFePO_4$, LFP) cathode. There are several qualitative differences from the system illustrated in Fig. 1. The particles are not spherical and an electronically conducting carbon-based binder layer is shown. The Li-ion-conducting electrolyte solvent is still assumed to be an organic liquid. However, the charge-transfer chemistry is different.

Figure 3 shows an expanded view at the cathode-particle scale. As illustrated, the charge transfer involves three phases — Li^+ in the electrolyte phase, Li in the LFP phase, and electrons in the carbon-based binder phase. As illustrated in the expanded balloon, the charge-transfer process and the Li reactions within the lithium-iron-phosphate cathode phase involve several chemical and physical processes. Thus, unlike Reaction 1 which involves two phases, the cathode chemistry in Fig. 3 involves three phases. As discussed subsequently, this difference has significant ramifications on representing the net charge-transfer process.

An LFP cathode particle behaves quite differently from a metal-oxide (e.g., Li_xCoO_2) cathode particle. The metal-oxide particles react with Li in a diffusive intercalation process, but the LFP particle is a phase-transformation electrode. As the Li is transported within the particle, a sharp phase-transformation front proceeds within the particle. So, rather than thinking about a spatially distributed Li fraction (e.g., Li_xCoO_2) within the particle, locations within the cathode particles are either $FePO_4$ or $LiFePO_4$. Predicting the phase-front speed depends upon complex thermodynamic, transport, and electrochemical factors, which have substantial impacts on modeling [6, 20–24].

2.2. *Sodium batteries*

Figure 4 illustrates a sodium-based battery, where the anode is molten Na, which also serves as the anode electronic conductor. There is no electrolyte within the anode structure. The separator, which is a solid ceramic Na^+ conductor (e.g., Nasicon), is thus also an electrolyte. The cathode compartment is composed of an electron-conducting carbon foam (electrode phase) and an aqueous iodine solution (electrolyte phase). The aqueous solution contains I_2, I^-, I^{3-}, and Na^+; the presence of multiple charge carriers represent complexity that is not well handled by standard transport models. At the interfaces between the carbon and the aqueous solution, charge transfer proceeds as

$$2I^-(\text{el}) \rightleftharpoons I_2(\text{el}) + 2e^-(\text{ed}). \tag{4}$$

Within the aqueous solution, homogeneous reaction can proceed as

$$I_2(\text{el}) + I^-(\text{el}) \rightleftharpoons I_3^-(\text{el}). \tag{5}$$

At the interface between the separator and the aqueous solution, Na^+ enters the aqueous solution at a rate that is needed to maintain charge neutrality within the cathode compartment. The Na^+ concentrations must be maintained below a precipitation limit where solid-phase NaI would be formed. Overall, the global chemistry can be represented as

$$2Na^+(\text{el}) + 2I^-(\text{el}) \rightleftharpoons 2Na(\text{ed}) + I_2(\text{el}). \tag{6}$$

However, it is evident that more complex chemistry and transport are present which support the global behavior.

2.3. *Lithium-based conversion batteries*

So-called "beyond lithium-ion' batteries include lithium-air (Li/O_2) and lithium-sulfur (Li/S) cells, which provide theoretical specific energies an order of magnitude above those of lithium-ion cells [26]. These batteries have conversion chemistries, that is, discharge/charge involves the formation and dissolution of bulk solid phases (lithium oxides, lithium sulfide, metallic lithium). The reaction mechanisms consist of multiple intermediate solid or dissolved species and a combination of parallel and sequential reaction pathways

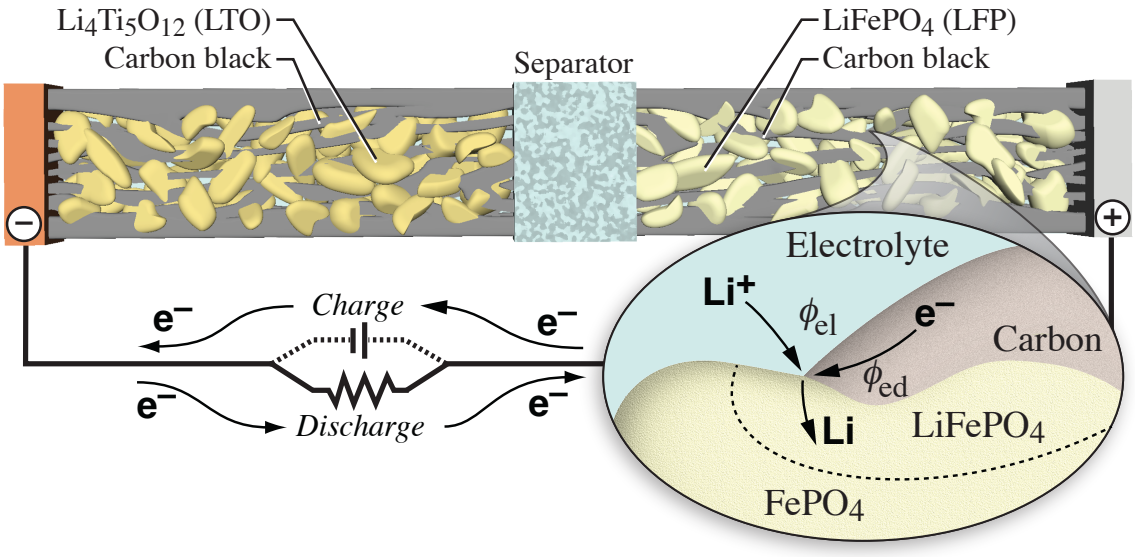

Figure 3: Illustration of chemical and transport processes in a Li-ion battery with a $Li_4Ti_5O_{12}$ anode, liquid electrolyte, and $LiFePO_4$ cathode.

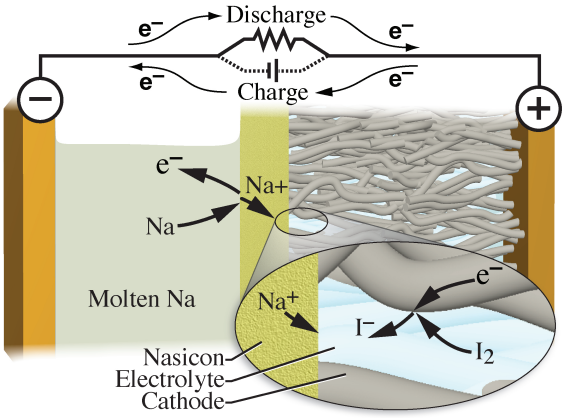

Figure 4: Illustration of a Na-based battery with a sodium-iodine cathode [25].

[27]. These multi-phase reactions can result in substantial volume changes within the electrode, which are not captured by standard modeling approaches [28]. Moreover, the associated kinetics are affected by nucleation and growth mechanisms [29], resulting in complex dependencies between reaction rate and morphology including particle size distributions [30].

Unlike most Li-ion battery models, which accommodate binary electrolyte salts such as Li^+ and PF_6^+, Li/S electrolytes have multiple polysulfide anion species whose reactive transport can result in cross-talk between the electrodes (so-called polysulfide shuttle) [31]. Many transport models for electrochemical cells, as discussed in Section 5, rely on significant simplifications that are only suited for binary solutions [16, 12]. Obviously, the modeling of transport in Li/S electrolytes (or similarly in the Na battery catholyte) requires models with the additional complexity of homogeneous reactions within the liquid catholyte.

The foregoing examples illustrate some differences and commonalities for different battery types. There are numerous other types of batteries, all of which have unique features and associated chemical and electrochemical complexities. The intent here is not to explore all battery architectures and chemistries, but rather to call attention to the need for generalized, flexible, electrochemistry modeling capabilities.

2.4. Solid-oxide fuel cells

As with batteries, there are numerous types of fuel cells. Figure 5 illustrates aspects of a channel layout in a solid-oxide fuel cell. In this case, the dense electrolyte membrane is often a yttrium-doped zirconate (YSZ), which is an oxygen-ion O^{2-} conductor [33]. The anode structure is typically a Ni-YSZ cermet. For hydrocarbon fuel feeds to the anode, catalytic fuel reforming takes place within the porous anode support structure. Near the anode-membrane interface, charge-transfer chemistry produces H_2O as adsorbed H atoms react with the O^{2-} emerging from the dense membrane on three-phase boundaries, delivering electrons to the Ni and ultimately the external circuit. As discussed by Goodwin, et al. [34], the charge-transfer process involves several elementary steps. Gas-phase O_2 is dissociately adsorbed onto the cathode surface and then electrochemically reduced with electrons returning from the external circuit. The resulting O^{2-} ions are incorporated from the cathode surface into the dense membrane.

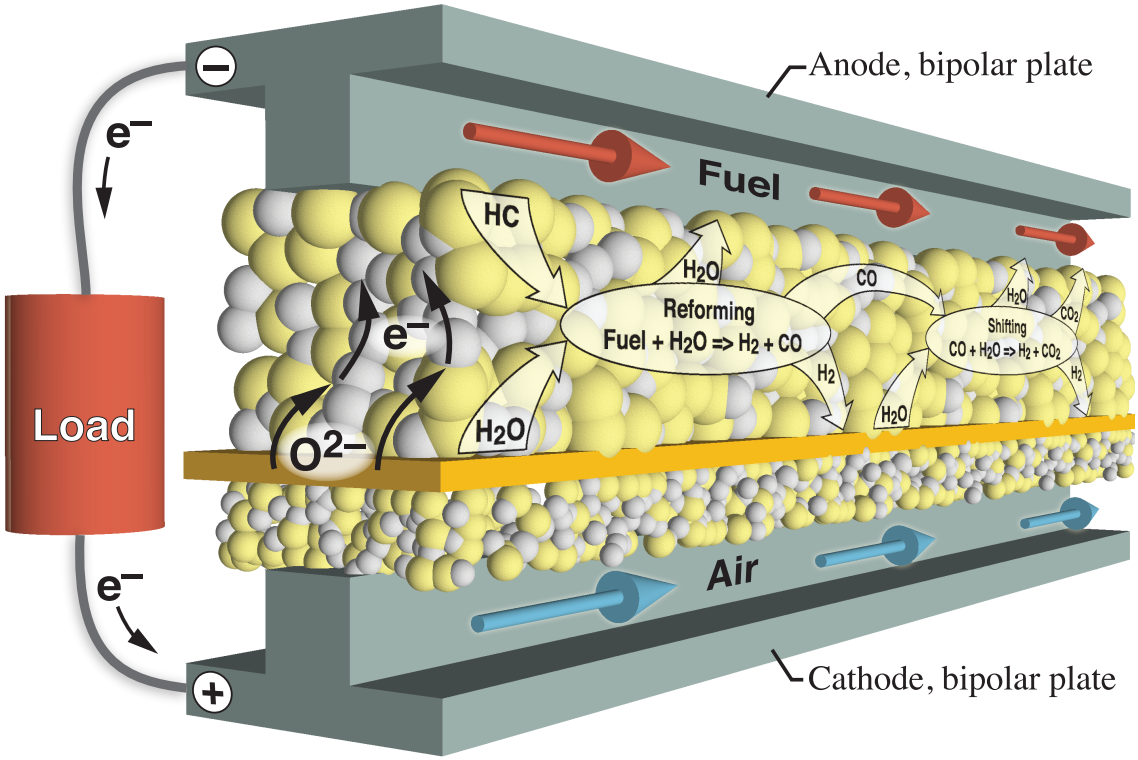

Figure 5: A solid-oxide fuel-cell channel operating on a hydrocarbon fuel, with internal reforming within the anode support structure.

Along the length of the fuel flow channel in the anode, the fuel is depleted and diluted with product H_2O and CO_2. Along the length of the air flow channel in the cathode, O_2 is removed from the air. The decreases in anode fuel and cathode O_2 concentrations along the length of the channel reduce the chemical potential driving force across the oxide-ion conducting membrane that provides for the cell voltage and facilitates current via electron production at the anode and consumption at the cathode. At operating conditions along the flow path where cell voltages fall below about 0.6 V, Ni in the porous anode structure begins to oxidize to NiO, leading to irreversible damage. Modeling Ni oxidation represents an example of electrochemical complexity that requires modeling structures that are not readily demonstrated in past modeling studies.

2.5. *Protonic-ceramic fuel cells*

Protonic-ceramic fuel cells (PCFC) [35, 32], as illustrated in the membrane-electrode assembly image in Figure 6, incorporate solid-oxide electrolytes made of materials such as yttrium-doped barium zirconate (e.g., $BaZr_{0.8}Y_{0.2}O_{3-\delta}$, BZY20). The BZY20 predominantly conducts protons, but is a mixed ionic-electronic conductor (MIEC) that has at least three mobile charged defects – protons $OH_O^{\bullet}$, oxide vacancies $V_O^{\bullet\bullet}$, and small polarons $O_O^{\bullet}$ [36]. The composite electrodes are porous structures that usually involve two solid phases and the gas phase flows of reactants. Like SOFCs, the anode is a cermet composite, with Ni being the electrode phase and BZY20 being the electrolyte phase. Such fuel cells are designed to operate on fuel streams of a hydrocarbon (e.g., natural gas) and steam.

In the anode of a hydrocarbon-fueled PCFC, steam reforming produces H_2, which reacts at the anode-electrolyte interface to deliver protons into the dense electrolyte membrane. The protons are transported across the dense membrane, where they react with adsorbed oxygen on the cathode to produce H_2O. PCFCs can convert hydrocarbons to electricity with high efficiency at temperatures in the range of 600 °C. [37–40]

The expanded balloon of Fig. 6 illustrates several heterogeneous and electrochemical reactions in a PCFC anode. Charge transfer can proceed at the three-phase boundaries formed at the intersections of the Ni, BZY20, and gas. Charge transfer can also proceed at the two-phase boundaries between the Ni and BZY20 phases. Charged defects (protons, vacancies, and polarons) from the charge-transfer reactions are incorporated into the MIEC electrolyte at the interfaces. The defect-incorporation reactions are not considered

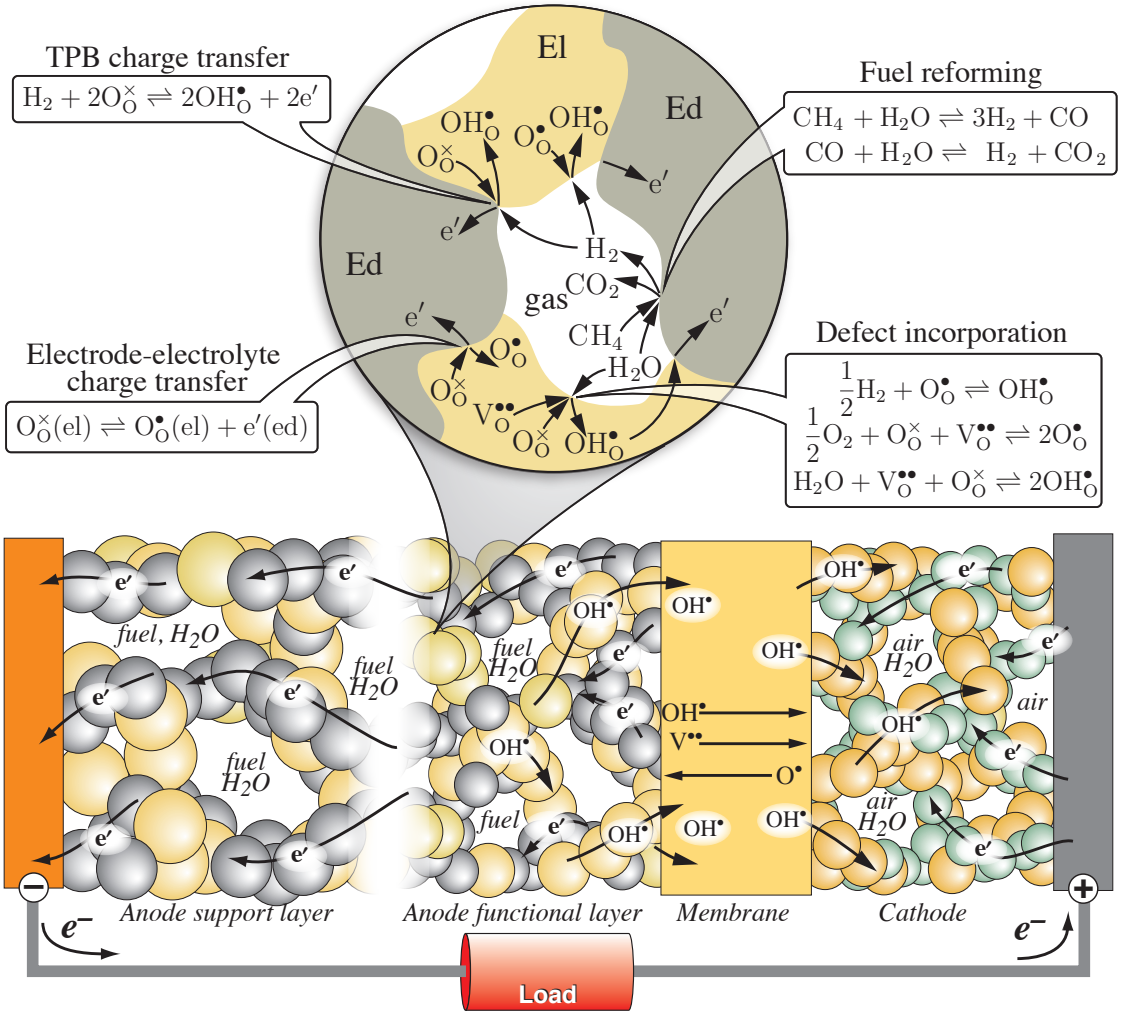

Figure 6: Illustration of the membrane-electrode assembly of a protonic-ceramic fuel cell [32].

as charge-transfer reactions because they do not transfer charge between two phases at different electrostatic potentials. In other words, all the charged defects are within the electrolyte phase; the gas phase species are charge-neutral. Finally, in addition to acting as the electron-conducting electrode phase, the Ni acts as a steam-reforming catalyst that facilitates the reactions of H_2O and hydrocarbons to form H_2, CO, and CO_2.

This PCFC example highlights a variety of chemical and electrochemical kinetics responsible for fuel-cell functionality. The MIEC nature of the electrolyte adds complexity to the chemistry and the transport that encourages the development for more robust modeling frameworks for fuel cell and electrochemical device modeling.

2.6. *Electrochemical membrane reactors*

Figure 7 illustrates a tubular cell that combines steam reforming, hydrogen separation, and hydrogen electrochemical compression. Such a system has been reported recently by Malerød-Fjeld, et al. [41]. In this system, methane and steam are introduced via a central feed tube, with reactive gases flowing through the annular space between the feed-tube exterior and the inner surface of a porous ceramic-metallic (cermet) tube support structure. The cermet here is similar to the PCFC and composed of Ni and BZY, with the Ni serving as both a reforming catalyst and an electron conductor. In this regard, the porous cermet anode functions similarly to the fuel-cell electrode illustrated in Fig. 6.

The catalytic reforming chemistry involves multiple surface reaction steps. Although much of the fuel-cell literature uses only two global reaction steps (one re-

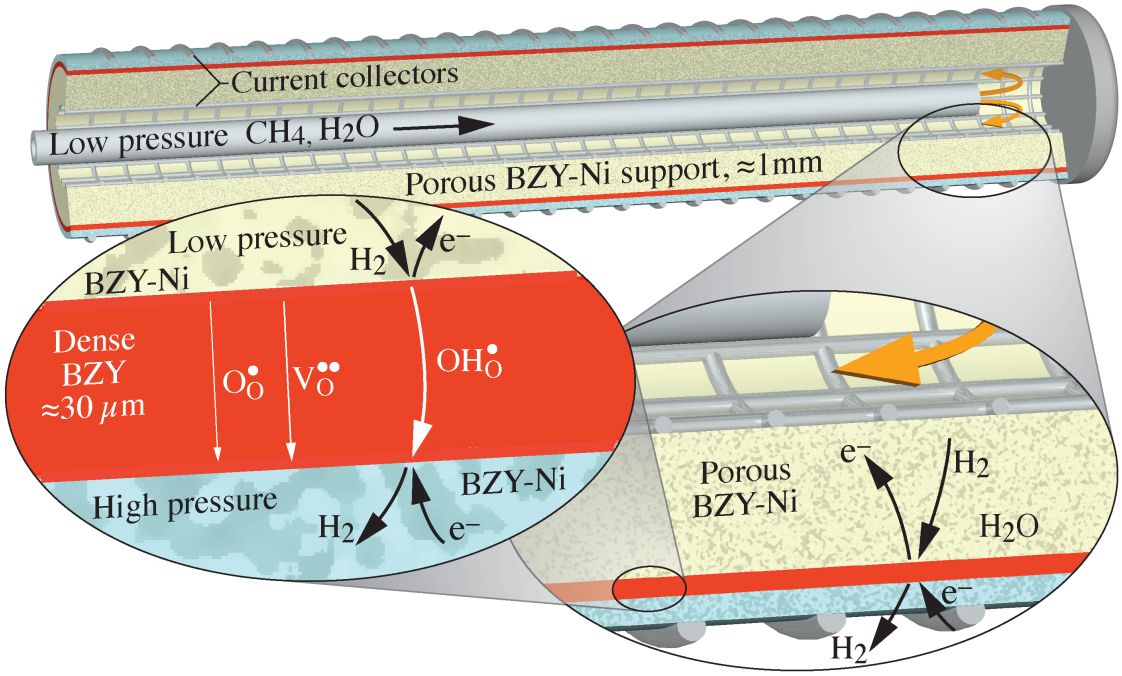

Figure 7: A tubular protonic-ceramic electrochemical cell that integrates steam reforming, hydrogen separation, and hydrogen compression.

forming and one water-gas shift), higher fidelity models use over 20 elementary reactions [33, 42, 43]. Thus, software that handles complex electrochemistry must interact effectively with comparable modeling capabilities that deal with complex homogeneous and heterogeneous thermal chemistry.

A thin (order tens of microns) and dense BZY mixed-conducting membrane is applied to the outside of the relatively thick (order few hundreds of microns) cermet support structure. The BZY membrane predominantly conducts protons ($OH^{\bullet}_{O}$), but other mobile charged defects include oxide vacancies ($V^{\bullet\bullet}_{O}$) and O-site small polarons ($O^{\bullet}_{O}$) [36]. Upon electrical polarization (typically, a few volts), protons are transported through the membrane. If the tube assembly is within a pressure vessel, the H_2 emerging from the membrane can be compressed.

As an ion conductor, the BZY membrane has relatively high resistance and thus ohmic heating must be dissipated within the membrane when operating at high current densities. The conductivity varies exponentially with temperature. With operating temperatures around 600 °C, practical devices must incorporate thermal balances for operational strategies that control membrane temperatures.

Other chemical processes can be accomplished using proton-conducting tubular assemblies such as illustrated in Fig. 7. For example, methane dehydroaromatization (MDA) is a pyrolytic process that synthesizes benzene from methane (i.e., $6CH_4 \rightleftharpoons 9H_2 + C_6H_6$). Because the process is equilibrium limited, removing H_2 through the membrane should, in theory, increase benzene yield [44, 42, 45, 43]. Of course, the catalytic MDA chemistry differs from steam-reforming chemistry with a higher propensity for solid carbon deposition and bifunctional catalysts with multiple reactive site types. Such complex chemistry coupled to the MIEC behavior of the proton-ceramic membrane strains the capabilities of most electrochemical and catalysis modeling frameworks at the reactor scale. As such, this indicates the need for new software tools with generalized data structures to enable modeling of electrochemical membrane reactors for chemical manufacturing.

3. Phases and phase interfaces

All electrochemical cells depend on the reactive transfer of charged species between electronically conductive electrodes and an ion-conducting electrolyte. The anode produces electrons by extracting charge from the conductive ion in the electrolyte, and the cathode consumes electrons to produce ions via a reduction reaction, often either of an oxide material (as in a Li-ion battery discharging) or of oxygen gas flow (as in a fuel cell cathode). Charge-transfer reactions occur at the electrode-

electrolyte interface where the two phases are at distinct electrostatic potentials (i.e., voltage Φ_m where m represents the phase). The charge transfer rate is related to the difference in Φ_m across phase interfaces and to the reactive species chemical potentials (μ_k were k represents the species). Since the electrodes and electrolytes are often dense solid or liquid phases, effective electrochemical modeling must incorporate non-ideal thermodynamics to properly account for μ_k. Depending on the direction of charge transfer current across the phase interface and the sign of the voltage change $\Delta\Phi$ across the phase interface, the cell either produces electrical work from the chemical free energy or the cell requires electrical work to increase chemical free energy.

Modeling electrochemical kinetics necessarily involves attention to *phase* thermodynamics, in particular of the mobile and reactive species. Electrochemically neutral reactions may also proceed within each phase or at phase interfaces. However, electrochemical *charge-transfer* reactions must proceed at phase interfaces. The rates of charge-transfer reactions depend on electrostatic potentials of the participating phases at the phase interfaces. Moreover, as is the case for thermal reactions, charge-transfer rates also depend on temperature activation and the activities of participating species.

3.1. Thermodynamics

The relationship between phase voltages Φ_m and species chemical potential μ_k can be derived from equilibrium thermodynamics. Both reaction rates and species transport fluxes depend on differences in species electrochemical potentials $\tilde{\mu}_k$ which are typically written as a function of μ_k and Φ_m as follows:

$$\begin{aligned}\tilde{\mu}_k &= \mu_k + z_k F \Phi_m, \\ &= \mu_k^\circ + RT \ln\left(\gamma_k \frac{[X_k]}{\left[X_k^\circ\right]}\right) + z_k F \Phi_m,\end{aligned} \tag{7}$$

μ_k° are the standard-state chemical potentials at temperature T and a fixed reference species concentrations $\left[X_k^\circ\right]$, and $[X_k]$ are the actual species molar concentrations (kmol m^{-3}). The gas and Faraday constants are represented as R and F, respectively. The activity coefficients for the k species are represented as γ_k, which capture any non-ideal species interactions associated with a given phase, relative to the fixed reference state. The species charges and the phase electrostatic potentials for each of the k species are represented as z_k and $\Phi_{m,k}$, respectively. While this definition of electrochemical potentials is convenient and most commonly used, Newman correctly points out that the separation of the electrochemical potential into strictly chemical and electric portions is both arbitrary and unnecessary [12]. The approach in Eq. 7 assumes that Φ_m is independent from the chemical composition, which results in a particular form for the activity coefficients γ_k. Other equivalent forms can also be derived which do not rely upon that assumption, as outlined in Newman's representation of quasi-electrostatic potential [12]. That said, we will henceforth use the electrochemical potential relationship in Eq. 7, primarily due to the prevalence of its application in current literature, but with full knowledge that other forms are also allowable and at times possibly advantageous. In particular, careful attention is required in understanding the thermodynamic definitions of the electrostatic potential Φ_m for a particular model. This is addressed further in Section 5.

For a given electrode-electrolyte interface reaction i under equilibrium conditions with no net current across the interface, the equilibrium condition relates the $\tilde{\mu}_k$.

$$\sum_{k=1}^{K} \nu'_{ki} \tilde{\mu}_k = \sum_{k=1}^{K} \nu''_{ki} \tilde{\mu}_k, \tag{8}$$

where ν'_{ki} and ν''_{ki} are the forward and backward stoichiometric coefficients for reaction i, respectively. Substituting Eq. 7 into Eq. 8 provides a basis for relating equilibrium chemical potential and voltage differences across electrode-electrolyte interfaces. The equilibrium $\Delta\Phi_m$ across the phase interface is relatively straightforward when there is only one charge transfer reaction across the phase interface. When multiple charge transfer reactions are active at an interface, multiple equilbria equations must be solved simultaneously to find the equilibrium $\Delta\Phi_m$. The equilibrium $\Delta\Phi_m$ is referred to as the reversible half-cell voltage. The sum of the anode-electrolyte and cathode-electrolyte reversible half cell voltages gives the so-called reversible cell voltage.

The relationship between thermodynamics and cell voltages, chemical reaction rates, and transport-driving gradients requires software with effective models and data structures for calculating both μ_k° and γ_k for the various materials/phases in relevant electrochemical cells. The chemical potentials can be evaluated in terms of the local phase Gibbs free energy G as

$$\mu_k = \left.\frac{\partial G}{\partial n_k}\right|_{T,p,n_{j\neq k}}, \tag{9}$$

where n_k are the number of moles of species k used in evaluating G. The activity coefficients γ_k in solid, liquid, or high-pressure gas mixtures are related to the molar excess Gibbs free energy g^{E} due to species interactions or mixing as

$$n_{\mathrm{T}} g^{\mathrm{E}} = G - \sum_{k=1}^{K} n_k \left[\mu_k^\circ + RT \ln\left(\frac{[X_k]}{\left[X_k^\circ\right]}\right)\right], \tag{10}$$

where $n_T = \sum_k n_k$. The excess free energy g^E can be simplified to reveal the relationship to the activity coefficients γ_k as

$$n_T g^E = \sum_{k=1}^{K} n_k RT \ln(\gamma_k). \tag{11}$$

Individual species γ_k are now defined as the partial derivative of the excess free energy with respect to n_k.

$$RT \ln(\gamma_k) = \left.\frac{\partial(n_T g^E)}{\partial n_k}\right|_{T,p,n_{j\neq k}}, \tag{12}$$

For ideal gas conditions as expected in SOFC gas flows, $g^E = 0$ and thus all $\gamma_k = 1$. However, for high-pressure flows and condensed phases (such as solid ceramic or organic liquid electrolytes), accurate theoretical models for γ_k are required.

A challenge for generalized electrochemical device modeling tools is the development of robust, quantitative models for g^E and self-consistent databases for different solid materials and fluids derived from experiments and/or molecular material models. Many thermodynamic models (some empirical [9, 46] and some more fundamental) have been developed for liquid electrolytes, solid oxides, and other non-ideal materials. Some of these models are referenced in subsequent sections, but the importance of developing user-accessible material and fluid models for calculating γ_k remains a critical step for developing next-generation electrochemistry modeling tools.

Further complications to thermodynamics related to mechanical stress can impact electrochemical reaction rates and driving forces for species transport. Stress induced diffusion can become significant for a variety of solid materials [47] (e.g. phase transformation battery electrodes [48], intercalation electrodes [49], and MIEC ceramic membranes [50–52]). Stress induced diffusion is accommodated by adding a term to the species electrochemical potential [48–50]. For example, the species electrochemical potential for a solid accounting for hydrostatic stresses can be expressed as [53, 50]

$$\tilde{\mu}_k = \mu_k + z_k F \Phi_m - \Omega_k \sigma_h, \tag{13}$$

where Ω_k is the species partial molar volume, and σ_h is the hydrostatic stress. To resolve the hydrostatic stress, an additional stress-strain relation can be imposed on the system. One constraint proposed by Yang for systems in quasi-static equilibrium with no external force can be expressed as

$$\nabla^2 \left(\sigma_h + \frac{2E\Omega_k}{9(1-\nu)} [X_k] \right) = 0 \tag{14}$$

where E and ν are the Young's modulus and Poisson's ratio of the material, respectively [54]. The importance of mechanical stress on electrochemical cell voltages and reaction rates depends strongly on the volumetric expansion or contraction of phases with changes in point defect concentrations $[X_k]$. This issue has received increased attention, recently, for both batteries and high-temperature fuel cells.

3.2. Interfaces

Electrochemical processes may proceed at the so-called three-phase boundaries (intersections between electrode, electrolyte, and an electrically neutral phase), or at two-phase interfaces (intersections between electrode and electrolyte phases). For example, consider a composite solid-oxide fuel cell anode, typically a porous structure comprised of the electrode phase (e.g., Ni), electrolyte phase (e.g., YSZ), and the gas phase containing the fuel. Li-ion battery electrodes can also have three-phase boundaries. Such a cathode may be structured with the electrode phase (e.g., $LiFePO_4$), an electrolyte phase (e.g., liquid ethylene carbonate), and an electrically conductive carbon additive phase (see, e.g. the expanded view in Fig. 3. In such cases, species (possibly including electrons) in three phases, as well as the electrostatic potentials of the phases, contribute to the charge-transfer chemistry. Li-ion batteries are also modeled assuming charge transfer reactions proceed at two-phase interfaces. In such cases, the charge-transfer reactions proceed on the surface between the electrode and electrolyte. The rates depend on the species concentrations and phase electrostatic potentials. Addtionally, rates depend on the local electrode microstructure (i.e., total amount of surface area or three-phase boundary available). As noted in section 2.1, accurate microstructural representations are required to accurately predict charge transfer rates.

3.3. Phase management

Electrochemical cells are often modeled using a homogenization approach, where the components of an individual subdomain (e.g., a composite electrode) are not spatially resolved on a microscopic scale, but are described as continuum of superimposed phases. In such a setting, the phases are characterized by their respective volume fractions ε_m and densities ρ_m. In standard modeling approaches these properties are often (implicitly) assumed constant. However, this is generally not the case. In lithium-ion batteries, active materials change their density and expand or contract during intercalation. During aging, secondary phases (e.g., SEI) grow,

gases are formed, and liquid electrolyte is consumed. In Li/O_2 batteries, different lithium oxides are formed, taking up the space of gas-filled or liquid-electrolyte-filled pore space, eventually causing pore clogging. In PEM fuel cells, liquid water saturation dynamically depends on operating conditions. A generalized continuity equation for all phases in a continuum setting may be formulated as [28]

$$\frac{\partial(\rho_m \varepsilon_m)}{\partial t} = \sum_{k,m} \dot{\omega}_k W_k, \tag{15}$$

where the sum runs over all species of phase m and $\dot{\omega}_k$ is the rate of formation (kmol m^{-3} s^{-1}).

The density ρ_m generally depends on phase composition, and constitutive equations including their parameters are required to describe this dependency. For gas phases, the assumption of the ideal gas law,

$$\rho_m = \frac{p}{RT} \frac{1}{\sum_k Y_k / W_k}, \tag{16}$$

is valid for the conditions met in most electrochemical cells. Here ρ_m is the phase density, p the pressure, and Y_k and W_k the mass fraction and molecular weight of species k. The density of an ideal condensed phase can be calculated from species partial molar volumes Ω_k,

$$\rho_m = \frac{\sum_k X_k W_k}{\sum_k X_k \Omega_k}, \tag{17}$$

where X_k is the species mole fraction. Using these constitutive relationships, Eq. 15 predicts the dynamic change of volume fractions of each phase. The necessary condition $\sum_m \varepsilon_m = 1$ requires the assumption of either the presence of a compressible gas phase that accommodates volume changes, or the presence of a mobile fluid phase that is displaced upon volume changes, or the coupling to a mechanical model describing overall volume expansion.

4. Charge-transfer chemistry

Electrochemical reactions occur at phase interfaces where charge is transferred between phases that are at different electrostatic potentials Φ. In Li-ion batteries, where the chemical potential driving forces across the cell are derived from Li stored in the electrode structures, these phase interfaces typically involve two phases (e.g., the electrolyte and the electrode as in Reaction 1 for a battery anode). In fuel cells, where the chemical-potential driving forces are derived from gas or liquid flows in contact with electrode/electrolyte interfaces, the charge-transfer occurs at so-called three-phase boundaries at the intersection between the electrode, electrolyte, and the electrically neutral fluid phase (cf., Fig. 6). For example, consider a solid-oxide fuel cell composite anode that is a porous structure comprised of the electron conducting electrode (e.g., Ni), the ion-conducting electrolyte (e.g., YSZ), and the gas phase containing the fuel (e.g., H_2). The charge-transfer chemistry may be represented as

$$H_2(g) + O^{2-}(el) \rightleftharpoons H_2O(g) + V_O(el) + 2e^-(an), \tag{18}$$

where $H_2(g)$ is in the gas phase, $O^{2-}(el)$ is in the electrolyte phase, $H_2O(g)$ is in the gas phase, $V_O(el)$ is an oxide ion vacancy in the electrolyte phase, and $e^-(an)$ is in the Ni phase. Reaction 18 is a global reaction that simplifies a more complex multi-step reaction sequence [33, 55].

The rate of a charge-transfer reaction at a multi-phase interface, according to fundamental Marcus theory, depends on the electrostatic potential difference between the participating electrode and electrolyte phases. However, nearly all battery and fuel-cell models are based on the Butler–Volmer formulation using "overpotentials."

4.1. Marcus theory

The fundamental Marcus formulation is general and does not depend on simplifying assumptions. Consider a general reaction, including a charge-transfer reaction, as represented by

$$\sum_{k=1}^{K} \nu'_{ki} \chi_k^{z_k} \rightleftharpoons \sum_{k=1}^{K} \nu''_{ki} \chi_k^{z_k}, \tag{19}$$

where $\chi_k^{z_k}$ is the chemical symbol for the kth species with charge z_k. The subindices represent species k and reaction i, with K being the number of species involved in the reaction. One of the "species" may be an electron. Reactions may involve species that reside in different phases, such as electrode and electrolyte phases. Electrochemical charge-transfer reactions transfer charge between phases. By convention, reversible charge-transfer reactions are usually written such that the forward direction is the *anodic direction* (i.e., producing electrons). The backward direction is called *cathodic*, meaning that electrons are consumed.

A reaction's rate of progress can be written in terms of the difference between forward (anodic) and backward (cathodic) rates of progress q_i as

$$q_i = q_{fi} - q_{bi} = k_{fi} \prod_{k=1}^{K} a_k^{\nu'_{ki}} - k_{bi} \prod_{k=1}^{K} a_k^{\nu''_{ki}}, \tag{20}$$

where a_k are the activity concentrations of the participating species. Generally speaking, the activity concentration for the species in a particular phase are equal to the activity coefficient γ_k multiplied by a dimensionally-appropriate concentration. For bulk, three-dimensional fluids (gases, liquids, solids), the concentration is simply the molar concentration $[X_k]$. For surface-adsorbed species, the concentration equals the surface coverage $\Gamma_m\theta_{k,m}$, where $\theta_{k,m}$ is the site fraction for species k on the surface of phase m and Γ_m is the total available surface site density on phase m.

For a given rate of progress q_i for a charge transfer reaction i, the associated charge transfer current $i_{e,i}$ is:

$$i_{e,i} = q_i n_{e,i} F, \tag{21}$$

where $n_{e,i}$ is the number of electrons (or equivalent charge) transferred to the electrode by the reaction:

$$n_{e,i} = -\sum_{k=1}^{K_{\text{ed}}} \nu_k z_k, \tag{22}$$

summed over all the K_{ed} species in the electrode phase, including electrons. The sign convention is such that an anodic rate of progress (produces negative charge in the electrode) is considered a positive current, while a cathodic rate of progress results in $i_{i,e} < 0$.

The forward and backward rate expressions for each reaction i are written as

$$k_{\text{f}i} = k_{\text{f}i}^{\text{t}} \exp\left[-\beta_{\text{a}i} \sum_{k=1}^{K} \frac{\nu_{ki} z_k F \Phi_k}{RT}\right], \tag{23}$$

$$k_{\text{b}i} = k_{\text{b}i}^{\text{t}} \exp\left[+\beta_{\text{c}i} \sum_{k=1}^{K} \frac{\nu_{ki} z_k F \Phi_k}{RT}\right], \tag{24}$$

where $\nu_{ki} = \nu''_{ki} - \nu'_{ki}$, and the forward and backward thermal rate coefficients (i.e., at zero electric-potential difference) are represented as $k_{\text{f}i}^{\text{t}}$ and $k_{\text{b}i}^{\text{t}}$. Assuming an elementary single-electron-transfer reaction, the anodic and cathodic symmetry factors $\beta_{\text{a}i}$ and $\beta_{\text{c}i}$ respectively are related by $\beta_{\text{a}i} + \beta_{\text{c}i} = 1$. There can be confusion between the anodic and cathodic symmetry factors (β_{a} and β_{c}) and the anodic and cathodic transfer coefficients (α_{a} and α_{c}). These coefficients are interchangeable for elementary, single-charge transfer reactions. For global reactions and reactions involving the transfer of more than one charge, the anodic and cathodic transfer coefficients (α_{a} and α_{c}) should be used because they are not constrained to sum to unity [56, 33, 57].

When there is a transfer of charge between phases at different electric potential, the term $\sum_{k=1}^{K} \nu_{ki} z_k F \Phi_k$ is non-zero, and the charge transfer rate is modified by the electric-potential difference between the two participating phases. Each phase m is assumed to be at an electric potential Φ_m. However, as a matter of convenience in computational implementation, each species can be assigned the charge associated with its phase. In other words, in writing Eqs. 23 and 24, each species k is assigned with an electric potential Φ_k, not the phase Φ_m directly. Generally, each species assumes the electric potential of phase in which it exists. The gas-phase is usually considered to be electrically neutral ($\Phi_m = 0$).

If all the charged species in an electrochemical reaction are in the same phase, the electric potentials do not affect the reaction rate (i.e., the exponential factors in Eqs. 23 and 24 are exactly unity). For example, consider the reaction $I_2 + I^- \leftrightharpoons I_3^-$, which may occur within a sodium battery aqueous electrolyte (i.e., a single phase). In this case, assuming Φ_k is the same for all species, $\sum_k \nu_k z_k = \nu_{I_2} z_{I_2} + \nu_{I^-} z_{I^-} + \nu_{I_3^-} z_{I_3^-} = (-1) \times (0) + (-1) \times (-1) + (+1) \times (-1) = 0$.

The thermal reaction rate expressions k_i^{t} ($k_{\text{f}i}^{\text{t}}$ or $k_{\text{b}i}^{\text{t}}$) are usually represented using the modified Arrhenius expression as

$$k_i^{\text{t}} = A_i T^{n_i} \exp\left(-\frac{E_i}{RT}\right), \tag{25}$$

where E_i represents the activation energy, A_i the pre-exponential factor, and n_i the temperature exponent. To satisfy microscopic reversibility and maintain thermodynamic consistency, the thermal component of the backward (cathodic) rate $k_{\text{b}i}^{\text{t}}$ is related to the forward (anodic) rate $k_{\text{f}i}^{\text{t}}$ via the reaction equilibrium constant K_i as

$$K_i = \frac{k_{\text{f}i}^{\text{t}}}{k_{\text{b}i}^{\text{t}}} = \exp\left(-\frac{\Delta G_i^\circ}{RT}\right) \prod_{k=1}^{K} \left[X_k^\circ\right]^{-\nu_{ki}}, \tag{26}$$

where ΔG_i° is the change of the standard-state Gibbs free energy for the reaction. Evaluating ΔG_i°, and hence the equilibrium constant, requires quantitative thermochemical properties for all species in the reaction.

4.2. Charge-transfer transition state

For the sake of illustration, consider a charge-transfer reaction representing behavior at a solid-oxide fuel cell anode,

$$\text{H(a)} + \text{OH}^-\text{(e)} \rightleftharpoons \text{H}_2\text{O(a)} + \text{(e)} + \text{e}^-\text{(a)}. \tag{27}$$

The nomenclature (a) and (e) indicate the anode and electrolyte phases, respectively. In this reaction, H(a) and H_2O(a) are assumed to be adsorbates on the anode (e.g., Ni) surface. A hydroxyl ion on the electrolyte surface (e.g., YSZ) is represented as OH^-(e) and (e)

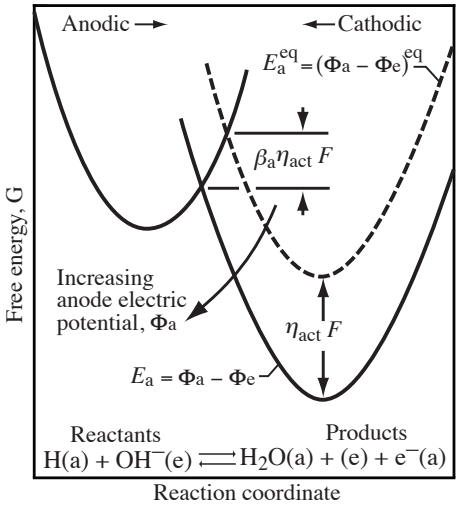

Figure 8: Potential energy surfaces to assist visualizing the effect of electric-potential difference on charge-transfer reaction rates.

represents an open site on the electrolyte surface. The electron $e^-(a)$ is in the electrode phase. Figure 8 illustrates potential-energy surfaces that assist understanding the influence of electric potentials on charge-transfer rates. The potential-energy surface on the left represents the reactants and the one on the right represents the products. The electric-potential difference at the interface between anode (a) and electrolyte (e) is written as $E_a = \Phi_a - \Phi_e$ (where the subscript 'a' represents that it is for the anode half-cell). The equilibrium electric-potential difference E_a^{eq} is the electric-potential difference at which the reaction proceeds at equal and opposite rates in the anodic (forward) and cathodic (backward) directions (illustrated as the dashed line). There is a potential-energy barrier between the reactant and product states, which tends to be cusp-like for charge-transfer reactions. When proceeding in the anodic direction, the charge-transfer reaction illustrated in Fig. 8 delivers electrons into the anode, which is at a lower electric potential than is the electrode. The electric potential difference therefore opposes the charge transfer reaction, in this state: the negatively charged electron is naturally repelled from the negative electrode. Some of the chemical energy stored as chemical bonds in the reactants is converted to electric current as electrons are delivered into the anode (i.e., the conduction band of the Ni). When the electrostatic potential of the anode increases relative to the electrolyte (i.e., E_a increases), the electrostatic barrier to charge transfer decreases.

The symmetry factors β are related to the magnitudes of the slopes of the potential-energy surfaces at their crossing point. Because the slopes are typically similar, the symmetry factors for elementary reactions are usually near $\beta = 1/2$. When the anode electric potential Φ_a is increased relative to the adjoining electrolyte electric potential Φ_e, the activation overpotential η_{act} is increased by the same amount. As illustrated in Fig. 8, the product-side potential energy surface is lowered by $\eta_{act}F$ and the anodic energy barrier is lowered by $\beta_a \eta_{act} F$. The energy barrier in the cathodic direction, meanwhile, increases by $(1 - \beta_a)\, \eta_{act} F$.

4.3. Butler–Volmer kinetics

The Bulter–Volmer formulation is an alternative approach to modeling charge transfer reactions. Fundamentally, the Bulter–Volmer expression can be derived from elementary Marcus Theory if there is a single rate-limiting charge-transfer reaction [8, 57]. Although the Butler–Volmer formulation is very widely used and has some significant advantages, it also has some very significant limitations. If the chemistry is represented simply as a single reaction (e.g., Reaction 1), then the limitations are not demanding. In fact, for such simple chemistry, there is relatively little need for generalized software. However, if the charge-transfer chemistry is a multi-step process, then the Butler–Volmer formulation is much less appropriate and more difficult to implement.

In the Butler–Volmer form, the charge-transfer current can be expressed as

$$\begin{aligned} i_e &= q_i n_{e,i} F \\ &= i_0 \left[\exp\left(\frac{\alpha_a F \eta_{act}}{RT} \right) - \exp\left(\frac{-\alpha_c F \eta_{act}}{RT} \right) \right], \end{aligned} \tag{28}$$

where i_e is the current at the electrode/electrolyte interface, $n_{e,i}$ is as in Eq. 22, i_0 is the exchange current density, and α_a and α_c are the anodic and cathodic transfer coefficients, respectively. The activation overpotential η_{act} is defined as

$$\eta_{act} = (\Phi_{ed} - \Phi_{el}) - (\Phi_{ed} - \Phi_{el})^{eq}, \tag{29}$$

where Φ_{ed} and Φ_{el} are the electrostatic potentials in the electrode and electrolyte phases, respectively. The term $E^{eq} = (\Phi_{ed} - \Phi_{el})^{eq}$ represents the equilibrium electrostatic-potential difference (cf., Section 4.4).

As expressed by Eq. 29, the Butler–Volmer formulation references electrostatic potentials to equilibrium reversible potential differences. At first, this may seem indirect and cumbersome. However, the advantage is that open-circuit voltages can be easily measured and, in many cases, evaluated theoretically. However, as discussed subsequently, as the chemistry becomes more complex, there are limitations and complications associated with the Butler–Volmer formulation.

The Butler–Volmer exchange current density i_0 includes the activities of the participating species. For example, the exchange current density for Reaction 1 at a graphite anode is typically represented as

$$i_0 = k_{ct} F [\mathrm{Li^+(el)}]^{\alpha_a} [\mathrm{Li_{max}(ed) - Li(ed)}]^{\alpha_a} [\mathrm{Li(ed)}]^{\alpha_c}. \tag{30}$$

Several important points can be noted about Eq. 30. The factor k_{ct} represents an Arrhenius rate expression that captures the temperature dependence and F is the Faraday constant. The exponents α_a and α_c are the anodic and cathodic symmetry factors, multiplied by the stoichiometric coefficients for the reaction, which are equal to unity in Reaction 1. The concentration $[\mathrm{Li_{max}(ed)}]$ represents the maximum concentration of intercalated Li within the graphite anode, which must be independently specified.

Strictly speaking, as stated, Reaction 1 means that the anode is Li metal. Although a bulk Li metal anode is a viable possibility, the common intent is that the anode is graphite with intercalated Li. So, the more correct way to state the reaction is

$$\mathrm{LiC_6(ed) \rightleftharpoons Li^+(el) + e^-(ed) + C_6(ed)}, \tag{31}$$

which explicitly identifies the fact that the anode is graphite and that the Li is intercalated. In this case, the exchange current density can be evaluated directly in the dilute solution approximation as

$$i_0 = k_{ct} F [\mathrm{Li^+(el)}]^{\alpha_a} [\mathrm{C_6(ed)}]^{\alpha_a} [\mathrm{LiC_6(ed)}]^{\alpha_c}. \tag{32}$$

The concentration $[\mathrm{LiC_6(ed)}]$ represents the intercalated Li and $[\mathrm{C_6(ed)}]$ represents the unoccupied graphite that is available to accept Li. The activity coefficients here are assumed to be unity and do not include complex concentrated solution effects [9, 58] . In this form, the identity of the electrode phase and its associated thermodynamics are clear in the reaction statement itself. Thus, these parameters do not need to be specified separately and software can be written to establish the form of the exchange current density.

4.3.1. Multi-step charge-transfer processes

Assuming there is a single rate-limiting reaction step, a multi-step charge transfer reactions can be written in Butler–Volmer form. However, the resulting exchange current density can become complex and not easily derived from the original reaction mechanism. Consider, for example, oxygen reduction at a protonic-ceramic fuel cell (PCFC) cathode. With very few exceptions in the literature, fuel cell models represent the cathode chemistry globally (in Kröger–Vink notation) as

$$\frac{1}{2}\mathrm{O_2(g)} + 2\mathrm{OH_O^\bullet(el)} + 2\mathrm{e'(ed)} \rightleftharpoons 2\mathrm{O_O^\times(el)} + \mathrm{H_2O(g)}, \tag{33}$$

where $\mathrm{OH_O^\bullet}$ is a proton in the electrolyte phase, $\mathrm{O_O^\times(el)}$ is an oxide ion in the electrolyte phase, e′ is an electron in the electrode (cathode) phase, and $\mathrm{O_2(g)}$ and $\mathrm{H_2O(g)}$ are gas-phase oxygen and steam respectively. Such a reaction is easily represented in Butler–Volmer form. However, assume that the actual chemistry is a multistep process as

$$\mathrm{O_2(g) + 2(s) \rightleftharpoons 2O(s)}, \tag{34}$$

$$\mathrm{OH_O^\bullet(el) + O(s) + e'(ed) = OH(s) + O_O^\times(el)}, \tag{35}$$

$$\mathrm{OH_O^\bullet(el) + OH(s) + e'(ed) = H_2O(s) + O_O^\times(el)}, \tag{36}$$

$$\mathrm{H_2O(s) = H_2O(g) + (s)}, \tag{37}$$

where O(s), OH(s), and $\mathrm{H_2O(s)}$ are the adsorbed oxygen, hydroxyl and water molecules on the cathode surface, respectively, and (s) is an empty cathode surface site. The rates of such elementary reactions can be represented according to Eqs. 20–24. Assuming a single rate-limiting charge-transfer step (e.g., Reaction 35), and with a great deal of tedious algebra, a Butler–Volmer rate expression can be derived [32]. Without going into details here, the resulting expression for the net current density is

$$i_e = i_0 \left[\exp\left(\frac{(1+\beta_{a,(35)}) F \eta_{act}}{RT} \right) - \exp\left(-\frac{\beta_{c,(35)} F \eta_{act}}{RT} \right) \right], \tag{38}$$

where the exchange current density may be expressed as

$$i_0 = i_0^* \frac{(p_{O_2}/p^*_{O_2})^{(1/2-\beta_{c,(35)}/4)} (p_{H_2O}/p^*_{H_2O})^{\beta_{c,(35)}/2}}{1 + (p_{O_2}/p^*_{O_2})^{1/2} + (p_{H_2O}/p^*_{H_2O})} \times [\mathrm{O_O^\times}]^{\beta_{c,(35)}} [\mathrm{OH_O^\bullet}]^{\beta_{a,(35)}}. \tag{39}$$

In these expressions, $\beta_{a,(35)}$ and $\beta_{c,(35)}$ are the symmetry factors associated with the rate-limiting charge-transfer reaction (Reaction 35). Note that the effective Butler–Volmer symmetry factors $(1+\beta_a)+\beta_c \neq 1$. The variables $p^*_{O_2} = 1/K_{34}$, $p^*_{H_2O} = 1/K_{37}$, are derived from equilibrium constants of the adsorption reactions. The variable i_0^* is an empirical parameter, which contains information such as three-phase-boundary length. Clearly, the resulting Butler–Volmer expressions are not easily derived from the reactions themselves.

Table 1: Proposed SEI film growth reaction mechanism for a graphite particle [11].

Graphite-SEI interface
$C_3H_4O_3(E) + (S^s) \rightleftharpoons C_3H_4O_3(S^s)$
$Li^+(S^s) \rightleftharpoons Li^+(E) + (S^s)$
$C_2H_4(E) + 2(S^s) \rightleftharpoons C_2H_4(S^s)$
$C_3H_4O_3^-(S^s) \rightleftharpoons C_3H_4O_3(S^s) + e^-_{S^b}$
$C_2H_4(S^s) + CO_3^{2-}(S^s) \rightleftharpoons C_3H_4O_3^-(S^s) + e^-_{S^b} + 2(S^s)$
$CO_3^{2-}(S^s) + 2Li^+(S^s) + (S^b) \rightleftharpoons Li_2CO_3(S^b) + 3(S^s)$
$Li(S^b) + (S^s) \rightleftharpoons V^-(S^b) + Li^+(S^s)$
$Li^+_{S^b} + (S^s) \rightleftharpoons Li^+(S^s)$
SEI-electrolyte interface
$e^-_{S^b} \rightleftharpoons e^-_{C_6}$
$Li(C_6) + V^-(S^b) \rightleftharpoons Li(S^b) + e^-_{C_6} + (C_6)$
$Li(C_6) \rightleftharpoons Li^+_{S^b} + e^-_{C_6} + (C_6)$

To pick another example, consider the important problem solid-electrolye-interface (SEI) chemistry in Li-ion battery anodes. Although details of this chemistry are not well understood, there is certainly active numerical and experimental research to understand it [3, 11, 59–61]. Again, without developing the details here, Table 1 shows the reactions mechanisms analyzed by Colclasure, et al. [3, 11]. The only purpose for showing such reactions here is to emphasize the need for handling increasingly complex electrochemical kinetics.

4.4. Reversible potentials

The *reversible potential* for any charge-transfer reaction i can be thermodynamically evaluated as [57]

$$E_i^{\mathrm{REV}} = \frac{1}{n_{\mathrm{e},i}F}\sum_{k=1}^{K}\nu_{ki}\,\mu_k, \tag{40}$$

where the signs of stoichiometric coefficients ν_{ki} assume that the reaction is written in the anodic direction (i.e., producing electrons). Assuming that there is a single global charge-transfer reaction for both the anode and cathode half-cells, the full-cell reversible potential can be expressed as

$$E^{\mathrm{REV}} = E_{\mathrm{c}}^{\mathrm{REV}} - E_{\mathrm{a}}^{\mathrm{REV}}. \tag{41}$$

To be more explicit, for example, consider a polymer-electrolyte-membrane (PEM) fuel cell. Assuming that the cathode half-cell reaction (written in the anodic direction) can be expressed as

$$H_2O(\mathrm{g,c}) \rightleftharpoons 2H^+(\mathrm{el}) + \frac{1}{2}O_2(\mathrm{g,c}) + 2e^-(\mathrm{c}), \tag{42}$$

the reversible potential can be expressed as

$$E_{\mathrm{c}}^{\mathrm{REV}} = \frac{1}{2F}\left(-\mu_{H_2O(\mathrm{g,c})} + 2\mu_{H^+(\mathrm{el})} + \frac{1}{2}\mu_{O_2(\mathrm{g,c})}\right). \tag{43}$$

Similarly, assuming the anode half-cell reaction is expressed as

$$H_2(\mathrm{g,a}) \rightleftharpoons 2H^+(\mathrm{el}) + 2e^-(\mathrm{a}), \tag{44}$$

the reversible potential on the anode can be expressed as

$$E_{\mathrm{a}}^{\mathrm{REV}} = \frac{1}{2F}\left(-\mu_{H_2(\mathrm{g,a})} + 2\mu_{H^+(\mathrm{el})}\right). \tag{45}$$

The full-cell reversible potential is then

$$\begin{aligned} E^{\mathrm{REV}} &= \frac{1}{2F}\left(-\mu_{H_2O(\mathrm{g,c})} + \frac{1}{2}\mu_{O_2(\mathrm{g,c})} + \mu_{H_2(\mathrm{g,a})}\right), \\ &= -\frac{\Delta G^\circ}{2F} + \frac{RT}{2F}\ln\frac{p_{H_2(\mathrm{g,a})}p_{O_2,\mathrm{c}}^{1/2}}{p_{H_2O(\mathrm{g,c})}}, \end{aligned} \tag{46}$$

with

$$\Delta G^\circ = \mu^\circ_{H_2O} - \frac{1}{2}\mu^\circ_{O_2} - \mu^\circ_{H_2}. \tag{47}$$

In these expressions, $p_{k,\mathrm{c}}$ and $p_{k,\mathrm{a}}$ are the partial pressure of species k on the cathode and anode side, respectively. The change in standard-state Gibbs free energy ΔG° can be expressed using the equilibrium cathode-side gas composition,

$$\exp\left(\frac{-\Delta G^\circ}{RT}\right) = \frac{p_{H_2O(\mathrm{g,c})}}{p_{H_2(\mathrm{g,c})}p_{O_2(\mathrm{g,c})}^{1/2}}. \tag{48}$$

Keep in mind that the reversible potential is an inherently equilibrium concept. That is, the gas on both sides of the membrane is assumed to be in thermodynamic equilibrium.

Substituting Eq. 48 into Eq. 46 results in a simplified expression for the full-cell reversible potential as

$$E^{\mathrm{REV}} = \frac{RT}{2F}\ln\frac{p_{H_2(\mathrm{g,a})}}{p_{H_2(\mathrm{g,c})}}. \tag{49}$$

Importantly, for PEM fuel cells, assuming the membraned is a pure proton conductor, the reversible potential may be evaluated using only the gas-phase compositions in the anode and cathode chambers.

If the electrolyte membrane is a single-ion conductor, the reversible potential is equivalent to the open-circuit potential

$$E^{\mathrm{REV}} = E^{\mathrm{OCV}}. \tag{50}$$

The open-circuit potential is the (measurable) electric potential difference between the cathode and anode current collectors,

$$E^{\mathrm{OCV}} = \Phi_{\mathrm{c}} - \Phi_{\mathrm{a}}, \tag{51}$$

when no external circuit is attached (i.e., an infinite-resistance external circuit). In most, if not all, electrochemical devices (e.g., batteries, fuel cells, membrane

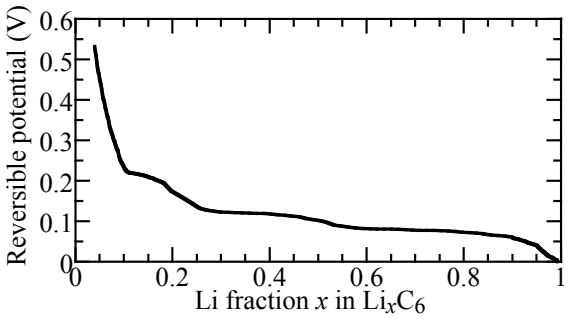

Figure 9: Reversible half-cell potential between an intercalating graphite electrode and Li metal.

reactors,...) the *open-circuit voltage* is easily measured. Thus, any practical model must be capable of accurately predicting open-circuit voltage.

If the reversible potential is known, either by theory or measurement, then including that information in modeling is valuable. In cases such as the PEM fuel cell, evaluating E^{REV} is straightforward in terms of gas-phase composition (cf. Eq. 49). However, in Li-ion batteries, for example, the situation is somewhat more complex. Figure 9 shows measurable half-cell reversible potential between a graphite anode and Li metal. The reversible potential varies as a function of intercalated Li (i.e., x in Li_xC_6). Such information can be communicated to a model via data fitting or theoretical expressions [9].

Expressing charge-transfer kinetics in the Butler–Volmer setting takes advantage of *a priori* knowledge of reversible potentials. Although the Butler–Volmer formulation depends on some very significant limiting assumptions, it does benefit from the inherent ability to predict measurable open-circuit voltages.

For membranes that are mixed ionic-electronic conductors (MIEC), in general $E^{\text{OCV}} \neq E^{\text{REV}}$. This is the case, for example, for protonic-ceramic fuel cells (PCFC) that are based on doped-perovskite membranes [35, 32]. In such cases, establishing the relationships between E^{OCV} and E^{REV} is more difficult. The doped-perovskite membranes typically have three or more charged defects, including small polarons that lead to so-called electronic leakage. Even at open-circuit (i.e., an infinite resistance external circuit), there is ionic and electronic transport through the membrane. In general, because of electronic leakage, $E^{\text{OCV}} < E^{\text{REV}}$. Models must be able to represent such behavior, which depends on mixed-conducting transport within the electrolyte membrane phase [62, 32].

4.5. Microscopic reversibility

Maintaining thermodynamic consistency and microscopic reversibility are important considerations in most, if not all, chemical kinetics modeling. It is important that the long-time (infinite time) result of kinetics approaches the thermodynamic equilibrium state. Achieving thermodynamic consistency requires knowing thermodynamic properties for all species participating in the kinetics. With known thermodynamic properties, the equilibrium state can be evaluated independently of any kinetics behavior by minimizing the Gibbs free energy. With gas-phase mixtures, the equilibrium composition is easily evaluated because the thermodynamics for most gas-phase species are readily available. In electrochemistry, the situation is quite different.

Consider an elementary electrochemical reaction mechanism, with the rates being expressed in the form of Marcus theory. Such mechanisms (e.g., Reactions 34–37) typically involve ionic species and surface adsorbates, the thermodynamic properties for which are largely unknown. If the thermodynamics are not known, then equilibrium state cannot be independently established from the thermodynamics (cf, Eq. 40). In electrochemistry, the equilibrium electrostatic potential differences at phase interfaces is an important aspect of the thermodynamic equilibrium. For applications such as batteries or fuel cells, predicting correct open-circuit potentials is a critically important aspect of a model. Thus, it is essential that a model using the Marcus formalism must have complete thermodynamic properties for all species.

In the Butler–Volmer setting, the reversible half-cell potentials can be specified independently. Then, the activation overpotentials are measured relative to the reversible potentials (Eq. 29). Thus, a model based on the Butler–Volmer formulation is inherently suited to respecting known reversible potentials and open-circuit potentials. However, the Butler–Volmer formulation depends on simplifying assumptions, some of which may not be consistent with the intent of the multi-step reaction mechanism. As reaction mechanisms become more complex, the Butler–Volmer formulation becomes increasingly cumbersome. Moreover, depending on details of the multi-step reaction mechanism, thermodynamic properties for individual species may be required to derive the Butler–Volmer exchange current densities. Thus, the potential value of the Butler–Volmer framework is diminished, and may be inappropriate.

The Marcus framework is certainly the most appropriate as the electrochemistry complexity increases. However, because the Marcus framework demands ther-

modynamic properties, there is a need to establish and validate the needed properties. Direct measurements, if possible, are difficult. Thus, there are opportunities for developing new atomistic-scale and *ab initio* simulation capabilities that are specifically targeted toward ionic species and surface adsorbates.

4.6. Macroscopic irreversibility

There are numerous examples where electrochemical cells show macroscopically irreversible features. In lithium-ion batteries, the SEI is observed to form at low anodic half-cell potentials, but does not completely decompose when going back to high potentials. Simple Tafel kinetics have been used to describe this behavior [63], which, however, clearly violate microscopic reversibility. In Li/O_2 batteries, charging typically proceeds at considerably higher overpotentials than discharge, leading to a strong asymmetry in the charge/discharge behavior [27]. In PEM fuel cells, observed open-circuit voltage is considerably lower than the value predicted by thermodynamics [64]. In all these cases, Butler-Volmer kinetics fail to describe the experimental observations. The understanding and prediction of macroscopic irreversibility remains a challenge for kinetic modeling.

5. Charge transport

As demonstrated, predicting charge-transfer reaction rates requires knowledge about the electrostatic potentials and species concentrations in participating phases. Both quantities are affected by the need to transport charged species to the relevant electrode-electrolyte interfaces. Transport of charged species may be modeled using dilute or concentrated solution theory. Phase electrostatic potentials may be modeled by solving a Poisson equation or by assuming strict electroneutrality.

As a practical matter, the much-simpler dilute approximation is the most widely used transport model. The dilute approximation usually leads to formulating problems in the context of Nernst–Planck fluxes. While considerably more accurate, the concentrated-solution theory is often applied in ways that are limited to binary systems, meaning only one cation and one anion. Transport within crystalline lattice structures typically must constrain the mobilities of charged defects to preserve site and charge balances at the lattice scale.

Generally, charged-species molar fluxes $\mathbf{J}_k$ can be represented as

$$\mathbf{J}_k = -u_k[X_k]\nabla\tilde{\mu}_k + [X_k]\,\mathbf{v}, \tag{52}$$

where u_k and $\mathbf{v}$ represent the ion mobilities and bulk phase velocity, respectively. Often, the bulk velocity is negligibly small, and certainly vanishes for solid electrolytes. Yet, in systems with strong volume changes within the composite electrode (e.g., Li/O_2 cells), bulk velocity may become important. Given a set of fluxes $\mathbf{J}_k$, the species concentrations can be expressed generally as a conserved quantity and integrated as a function of time:

$$\frac{\partial\,[X_k]}{\partial t} = -\nabla\cdot\mathbf{J}_k + \dot{\omega}_k. \tag{53}$$

Here $\dot{\omega}_k$ is a volumetric molar production rate. Additional relationships are needed to determine the electrostatic potentials Φ (cf., Section 5.1) and convective velocities $\mathbf{v}$. The current density within the phase can be expressed in terms of the charge-species fluxes as

$$\mathbf{i} = F\sum_k z_k\mathbf{J}_k. \tag{54}$$

5.1. Electroneutrality

Predicting the electrostatic potential fields is an essential element of all electrochemistry models. Requiring electroneutrality within a phase can be a practical and reasonably accurate assumption. Strict electroneutrality means that

$$\sum_k F z_k\,[X_k] = 0, \tag{55}$$

everywhere within the bulk phase. Strict charge neutrality can also be enforced as

$$\nabla\cdot\mathbf{i} = 0. \tag{56}$$

Equation 56 is typically referred to as *conservation of charge*. Although strict electroneutrality (or *conservation of charge*) can be a reasonably accurate approximation, it is not entirely correct. Rather, the electrostatic potential is more accurately governed by a Poisson equation as

$$\nabla\cdot(\varepsilon\nabla\Phi) = -\rho = -\sum_k F z_k\,[X_k]\,, \tag{57}$$

where ε is the phase's dielectric constant and ρ is the local charge density [12]. Interestingly, while Eq. 55 is roughly correct (i.e., $\sum_k F z_k\,[X_k] \approx 0$), it also is the case that

$$\nabla\cdot(\varepsilon\nabla\Phi) \neq 0. \tag{58}$$

In other words, assuming that $\nabla\cdot(\varepsilon\nabla\Phi) = 0$ is *incorrect*! As discussed by Bazant and colleagues [65], because typically $\varepsilon \ll 1$, small (second-order) variations in ρ lead to large (leading order) variations in Φ. When Eq. 57 is solved coupled together with

species-conservation equations (e.g., Eq. 53), the resulting models are called Nernst–Planck–Poisson (NPP) models [66].

Most electrochemistry models, at least those at the technology scale (e.g., batteries, fuel cells, etc.) assume a sharp "jump" in the electrostatic potential across phase boundaries. This jump $\Delta\Phi$ is used to evaluate electrochemical charge-transfer rates at the phase interfaces. However, by solving Eq. 57 on very small length scales near the phase interfaces, it is possible to resolve the electrical *double layers* at the phase boundaries. In other words, it is possible to resolve the electrostatic potential and species profiles within the extremely thin double layers. Nevertheless, at the technology level, there is usually no practical value to resolving the double-layer structure. Moreover, because of the enormous scale disparity, it is entirely impractical to resolve double-layer structure together with predicting larger-scale electrochemical performance.

5.2. Dilute solution theory

Dilute solution theory assumes that within an ionic solution, the charged species do not directly interact. The species flux can be expanded using the Nernst–Einstein equation ($D_k = RTu_k$) to

$$\mathbf{J}_k = -D_k \frac{\nabla(\gamma_k [X_k])}{\gamma_k} - D_k \frac{z_k F}{RT} [X_k] \nabla\Phi + [X_k]\mathbf{v}, \quad (59)$$

where D_k are species diffusion coefficients. For dilute solutions, the activity coefficients γ_k approach unity for all species [12], which results in:

$$\mathbf{J}_k = \underbrace{-D_k \nabla [X_k]}_{\text{diffusion}} \underbrace{-D_k \frac{z_k F}{RT} [X_k] \nabla\Phi}_{\text{migration}} + \underbrace{[X_k]\mathbf{v}}_{\text{convection}}. \quad (60)$$

The species fluxes are driven by diffusion and migration, and possibly convection.

Using Eq. 60, the current density, ionic conductivity, and transference numbers t_k can be derived [12]. The current density can be expressed as

$$\mathbf{i} = -F \sum_k z_k D_k \nabla [X_k] - F^2 \nabla\Phi \sum_k z_k^2 u_k [X_k] + F\mathbf{v} \sum_k z_k [X_k]. \quad (61)$$

The ionic conductivity σ is obtained in the limit of no concentration gradients and no bulk velocity,

$$\sigma = F^2 \sum_k z_k^2 u_k [X_k]. \quad (62)$$

The transference number t_k is defined as the fraction of current carried by species k within an electrolyte. Continuing to assume negligible concentration gradients and bulk velocity, the transference number can be expressed as

$$t_k \mathbf{i} = -F^2 z_k^2 u_k [X_k] \nabla\Phi = \frac{z_k^2 u_k [X_k]}{\sum_k z_k^2 u_k [X_k]} \mathbf{i}, \quad (63)$$

$$t_k = \frac{z_k^2 u_k [X_k]}{\sum_k z_k^2 u_k [X_k]}. \quad (64)$$

By definition, the transference numbers, when summed over all mobile ions in a phase, must sum to unity.

A central tenet of the dilute solution theory is that the flux of species k depends on diffusion coefficients and mobilities that are associated with species k alone. In the more general case, the fluxes depend on diffusion coefficient matrices that represent the binary molecular interactions between all species (i.e., off-diagonal Onsager contributions) [72, 90, 91].

5.2.1. Dilute solution binary electrolyte

Significant simplifications are possible for electrolytes that carry only two charged species. Assuming, for example, a liquid electrolyte solution composed of a salt that dissociates into one cation and one anion. Let ν_+ and ν_- be the number of cations and anions produced by dissolving electrolyte salt[1]. Assuming strict electroneutrality, the anion and cation concentrations ($[X_-]$ and $[X_+]$) within the electrolyte are related to the original salt concentration C as

$$C = \frac{[X_+]}{\nu_+} = \frac{[X_-]}{\nu_-}. \quad (65)$$

Assuming no homogeneous reactions within the solvent and no bulk velocity, the species continuity equation can be expressed as

$$\frac{\partial C}{\partial t} = \mathcal{D}\nabla^2 C, \quad (66)$$

where

$$\mathcal{D} = \frac{z_+ u_+ D_- - z_- u_- D_+}{z_+ u_+ - z_- u_-} \quad (67)$$

is called the *ambipolar* diffusion coefficient [12]. The diffusion coefficient can be simplified using the Nernst–Einstein equation ($D_k = RTu_k$) to

$$\mathcal{D} = \frac{D_+ D_- (z_+ - z_-)}{z_+ D_+ - z_- D_-}. \quad (68)$$

[1] Newman introduced a ± nonclature that is widely used. However, it is necessarily restricted to binary mixtures.

The ambipolar diffusion coefficient is used frequently in modeling solid-state ceramic electrolytes, where it is also called the *chemical diffusion coefficient*. Although the application is limited to dilute binary systems, the explicit consideration of the electrostatic potential is eliminated. The resulting mathematical problem can be treated as a relatively straightforward diffusion problem [66–68].

5.3. Concentrated solution theory

While dilute solution theory is convenient to implement in simulations, the basic assumption of non-interacting charged species quickly loses validity in many electrochemical systems, paricularly with liquid battery electrolytes. Moreover, as noted by Bizeray, et al. [92], the electric potential Φ in the Nernst-Planck formulation has a thermodynamic definition which does not readily allow experimental measurement and can thus lead to errors in experimentally-determined conductivities for individual charge carriers. A more accurate and fundamentally sound approach to transport modeling for such systems is the concentrated solution theory. The multicomponent transport for concentrated solution theory can be represented generally as

$$\begin{aligned}[X_k]\,\nabla\tilde{\mu}_k &= \sum_j K_{kj}\left(\mathbf{v}_j - \mathbf{v}_k\right)\\ &= \frac{RT\,[X_k]}{[X_T]}\sum_j \frac{\left[X_j\right]}{\mathcal{D}_{kj}}\left(\mathbf{v}_j - \mathbf{v}_k\right),\end{aligned} \tag{69}$$

where K_{kj} are the *friction coefficients* (also referred to as interaction coefficients), $[X_T] = \sum_k [X_k]$ is the total concentration, and $\mathcal{D}_{kj}$ are binary diffusion coefficients. By definition, the binary-diffusion-coefficient matrix is symmetric ($\mathcal{D}_{kj} = \mathcal{D}_{jk}$). The so-called self-diffusion coefficient $\mathcal{D}_{kk}$ can be evaluated, but has little or no physical utility. Equation 69 is analogous to the Stefan–Maxwell equations [69] and equivalent to those developed by Onsager [70, 12].

As discussed by Newman and Thomas-Alyea [12], concentrated solution theory (Eq. 69) is typically inverted to evaluate the diffusion velocities. The concentrated solution theory can be expressed as

$$[X_k]\,\nabla\tilde{\mu}_k = \sum_j M_{kj}\left(\mathbf{v}_j - \mathbf{v}_0\right), \tag{70}$$

where

$$M_{kj} = \begin{cases} K_{kj} & \text{if } k \neq j \\ K_{kj} - \sum_i K_{ki}, & \text{if } k = j. \end{cases} \tag{71}$$

The diffusion velocities can then be expressed as

$$\mathbf{v}_j - \mathbf{v}_0 = -\sum_{k\neq 0} L^0_{kj}\,[X_k]\,\nabla\tilde{\mu}_k, \quad j \neq 0, \tag{72}$$

where L^0_{kj} is evaluated as the inverse of the M^0_{kj} matrix as

$$L^0_{kj} = -\left(M^0_{kj}\right)^{-1}. \tag{73}$$

The submatrix M^0_{kj} is the matrix M_{kj} with the row and column of a reference species '0' removed. The species fluxes can be expressed as

$$\mathbf{J}_k = [X_k]\,\mathbf{v}_0 - \sum_{j\neq 0} L^0_{kj}\left[X_j\right][X_k]\,\nabla\tilde{\mu}_j. \tag{74}$$

The velocity of species '0' is such that the net diffusive flux vanishes. That is,

$$\frac{\sum_k \mathbf{J}_k W_k}{\sum_k [X_k]\,W_k} = \mathbf{v}, \tag{75}$$

where $\mathbf{v}$ is the bulk velocity and W_k is the molecular weight of species k. The current density can then be evaluated as

$$\begin{aligned}\mathbf{i} &= F\sum_k z_k\,[X_k]\,\mathbf{v}_k = F\sum_k z_k\,[X_k]\,(\mathbf{v}_k - \mathbf{v}_0),\\ &= -F\sum_{k\neq 0} z_k\,[X_k]\sum_{j\neq 0} L^0_{kj}\left[X_j\right]\nabla\tilde{\mu}_j.\end{aligned} \tag{76}$$

In a solution with spatially uniform species concentrations (i.e., $\nabla\tilde{\mu}_k = z_k F\nabla\phi$), the conductivity of the solution is

$$\sigma = -F^2\sum_{k\neq 0}\sum_{j\neq 0} L^0_{jk} z_j z_k [X_k][X_j], \tag{77}$$

and the transference number with respect to the reference species '0' is

$$t^0_k = \frac{z_k[X_k]F^2}{\sigma}\sum_{j\neq 0} L^0_{kj} z_j [X_j]. \tag{78}$$

It should be noted that the transference number for a concentrated solution *depends* on species '0'. Thus, unlike dilute solution theory, the transference number t^0_k is no longer analogous to the fraction of current carried by species k. The sum of the transference numbers must be unity, independent of the reference species '0' [12].

5.3.1. Concentrated solution binary electrolyte

A binary electrolyte is composed of a single anion species, a single cation species, and the solvent. The following analysis uses subscripts '+', '−', '0' to represent the anion, cation, and solvent, respectively. Concentrated solution theory for a binary electrolyte can be expressed as

$$\begin{aligned}[X_+]\,\nabla\mu_+ = {}& RT\frac{[X_+]\,[X_0]}{[X_T]\,\mathcal{D}_{+0}}\left(\mathbf{v_0} - \mathbf{v}_+\right)\\ &+ RT\frac{[X_+]\,[X_-]}{[X_T]\,\mathcal{D}_{+-}}\left(\mathbf{v}_- - \mathbf{v}_+\right),\end{aligned} \tag{79}$$

$$[X_-]\nabla\mu_- = RT\frac{[X_-][X_0]}{[X_T]\mathcal{D}_{-0}}(\mathbf{v_0}-\mathbf{v}_-) + RT\frac{[X_-][X_+]}{[X_T]\mathcal{D}_{-+}}(\mathbf{v}_+-\mathbf{v}_-), \tag{80}$$

The cation flux can be expressed as

$$\begin{aligned}\mathbf{J}_+ &= [X_+]\mathbf{v}_+ \\ &= \frac{1}{\mathcal{D}_{+-}[X_0]-\mathcal{D}_{+0}[X_-]}\left(\frac{[X_+][X_T]\mathcal{D}_{+-}\mathcal{D}_{+0}}{RT}\nabla\mu_+ \right. \\ &\quad \left. + [X_0][X_+]\mathcal{D}_{+-}\mathbf{v}_0 + [X_+][X_-]\mathcal{D}_{+0}\mathbf{v}_-\right).\end{aligned} \tag{81}$$

It can be shown that the anion flux, cation flux, current density, and transference number (Eqs. 54, 69 and 78) can be combined such that [71, 12]

$$\mathbf{J}_+ = \frac{[X_+][X_T]\mathcal{D}}{[X_0]RT(\nu_++\nu_-)}\nabla(\nu_+\mu_++\nu_-\mu_-) + \frac{\mathbf{i}t_+^0}{z_+F} + [X_+]\mathbf{v}_0, \tag{82}$$

$$\mathbf{J}_- = \frac{[X_-][X_T]\mathcal{D}}{[X_0]RT(\nu_++\nu_-)}\nabla(\nu_+\mu_++\nu_-\mu_-) + \frac{\mathbf{i}t_-^0}{z_-F} + [X_-]\mathbf{v}_0, \tag{83}$$

where $\mathcal{D}$ is the diffusion coefficient 'based on the thermodynamic driving force' and is similar to the dilute-solution diffusion coefficient (see Eq. 68)

$$\mathcal{D} = \frac{\mathcal{D}_{0+}\mathcal{D}_{0-}(z_+-z_-)}{z_+\mathcal{D}_{0+}-z_-\mathcal{D}_{0-}}. \tag{84}$$

The cation transference number for a binary concentrated solution is expressed as

$$t_+^0 = \frac{z_+\mathcal{D}_{0+}}{z_+\mathcal{D}_{0+}-z_-\mathcal{D}_{0-}}. \tag{85}$$

The diffusion coefficient for concentrated solutions is usually measured based on the gradient of concentration

$$D = \mathcal{D}\frac{[X_T]}{[X_0]}\left(1+\frac{d\ln\gamma_\pm}{d\ln m}\right), \tag{86}$$

where $\gamma_\pm$ is the mean molal activity coefficient and m is the molality [12, 71, 72]. The species continuity equations (assuming no bulk velocity or homogeneous reactions) can then be combined using strict electroneutrality as

$$\frac{\partial C}{\partial t} = \nabla\cdot\left[D\left(1-\frac{d\ln[X_0]}{d\ln C}\right)\nabla C - \frac{\mathbf{i}\,t_+^0}{z_+\nu_+F}\right]. \tag{87}$$

5.4. Binary diffusion coefficients in liquids

There are several approaches to approximating the binary diffusion coefficients in liquids, with the Stokes–Einstein relationship being widely used. However, the Stokes–Einstein relation is most accurate for infinitively dilute systems. Empirical relationships to modify the Stokes–Einstein relationship have been developed to more accurately predict the binary diffusion coefficients in dilute systems. In concentrated solutions, experimental studies have shown that the binary diffusion coefficients depend on concentrations, temperatures, and viscosities [69].

In concentrated solutions, electrical interactions strongly influence ion mobility [73, 74]. In accordance with the Debye–Hückle theory, ions tend to form "ion atmospheres" that can increase or decrease mobility of charged species due to positive and negative charge interactions.

5.4.1. Stokes–Einstein binary diffusion coefficients

The Einstein diffusion equation can be stated generally as

$$\mathcal{D}_{kj} = \frac{k_\mathrm{B}T}{\zeta}, \tag{88}$$

where k_B is the Boltzmann constant, T is temperature, and ζ is a friction coefficient [75, 73]. If the fluid is isotropic, incompressible, and Newtonian, and the boundary between the particles is fixed, high-shear, and nonslip, then Stokes's law for creeping flow states

$$\zeta = 6\pi\eta_j r_k, \tag{89}$$

where η_j is the fluid viscosity of species j and r_k is the molecular radius of species k. If the fluid is Newtonian and there is zero-shear between the particles, then the friction coefficient can be expressed as

$$\zeta = 4\pi\eta_j r_k. \tag{90}$$

If there is shear and slip between the particles, the friction coefficient can be expressed as

$$\zeta = 6\pi\eta_j r_k\left(\frac{2\eta_j+\upsilon r_k}{3\eta_j+\upsilon r_k}\right), \tag{91}$$

where υ is the sliding coefficient [76, 69, 75]. If there is high shear and no slip between the particles ($\upsilon\to\infty$), Eq. 91 simplifies to Eq. 89. If there is zero shear and high slip ($\upsilon\to 0$), Eq. 91 simplifies to Eq. 90.

The Stokes–Einstein relationships are most accurate for infinitively dilute concentrations. Theoretical adjustments for polar and non-circular molecules have

been proposed to modify the friction coefficient ζ [73]. Empirical relations modifying the Stokes–Einstein relation for infinitely dilute solutions have also been developed to add concentration, activity, and viscosity dependence [77]. In addition, the product of the binary diffusion coefficient involving the solvent and the viscosity η have been shown to be reasonably constant over moderate concentration ranges (e.g. $\eta\mathcal{D}_{k0}$ is constant) [69]. The binary diffusion coefficients between ions, according to Debye-Hückel-Onsager theory, is expected to be proportional to $\sqrt{C}$ [74, 72]. Additional theories for concentrated solutions have been developed to better describe concentrated solution performance [78, 79, 91]. Complex electrochemistry software must able to accommodate concentrated solution theories with varying levels of complexity, to reduce the computational burden placed on the software user.

5.5. *Charged transport in solids*

Broadly speaking, there are three approaches to model charge and species transport within solids. These approaches, in ascending order of complexity, are

- Solid phases with effective properties
- Dilute defect solids (negligible Onsager cross-diagonal coefficients)
- Concentrated defect solids (significant Onsager cross-diagonal coefficients)

Battery electrodes are commonly modeled using solid phase models with effective properties [9, 7, 48, 81, 82, 20]. Such models assume that the mobile solid-phase species is charge-neutral. Thus, the species transport and charge transport are no longer explicitly coupled. These models represent species fluxes as

$$\mathbf{J}_k = -D_{k,\text{eff}} \nabla \left(\gamma_k \left[X_k \right] \right), \tag{92}$$

and current density as

$$\mathbf{i} = -\sigma_{\text{eff}} \nabla \Phi. \tag{93}$$

In these expressions, $D_{k,\text{eff}}$ and σ_{eff} are the effective diffusion coefficients and the effective conductivity, respectively. The effective parameters can be functions of concentration, thus coupling the charge and species equations.

The differences between the dilute defect and concentrated solid methods can be viewed in the context of the Onsager matrix. The Onsager coefficients $L_{k,i}$ relate the electrochemical potentials of mobile species and their respective fluxes. Mathematically, this relationship can be expressed as

$$\begin{bmatrix} \mathbf{J}_1 \\ \vdots \\ \mathbf{J}_k \\ \vdots \\ \mathbf{J}_K \end{bmatrix} = \begin{bmatrix} L_{1,1} & L_{1,2} & \dots & L_{1,K} \\ \vdots & \vdots & \ddots & \vdots \\ L_{k,1} & L_{k,2} & \dots & L_{k,K} \\ \vdots & \vdots & \ddots & \vdots \\ L_{K,1} & L_{K,2} & \dots & L_{K,K} \end{bmatrix} \begin{bmatrix} \nabla\tilde{\mu}_1 \\ \vdots \\ \nabla\tilde{\mu}_k \\ \vdots \\ \nabla\tilde{\mu}_K \end{bmatrix}. \tag{94}$$

As derived by Osager and Fuoss [74], the Onsager coefficient matrix is symmetric. If the flux of species k is independent of other species, the off-diagonal Onsager coefficients $L_{k,i}$ vanish. The off-diagonal coefficients are negligible if the short-range and long-range interactions between charged species are negligible [83]. In this text the *dilute defect solids* are models that assume that all off-diagonal Onsager coefficients are negligible and conversely the *concentrated defect solids* assume that there are significant off-diagonal coefficients.

Dilute defect models are used when the solid-phase species are charged, but their mobilities are independent of other charged species. For *dilute defect solids* the flux of species k is the same as dilute solute solution theory with the bulk velocity being zero (cf., Eq. 60) [55, 50, 66, 36, 68, 32, 57].

Concentrated defect models are used when the solid-phase species are charged, and the species' mobilities depend on other charged species [83]. The resultant species fluxes, which are analogous to concentrated solution theory, can be expressed as

$$\mathbf{J}_k = \sum_i L_{k,i} \nabla\tilde{\mu}_i. \tag{95}$$

Equation 95 shows that the flux of species k depends on the electrochemical-potential gradients of all other species that have non-zero Onsager coefficients. Thus, the species transport equations are tightly coupled. The off-diagonal Onsager coefficients $L_{i,k}$ must be estimated or measured for every species pairing. In principle, these parameters can be measured using electron blocking electrodes and material blocking electrodes [84, 85]. However, because there are numerous potential species combinations, many Onsager coefficients need to be estimated.

5.5.1. *Lattice-scale site and charge balances*

In solid-phase crystalline electrolytes, models must be concerned with lattice-scale constraints. For example, consider strontium- and iron-doped lanthanum cobaltites, which can be generally represented as $La_{1-x}Sr_xCo_{1-y}Fe_yO_{3-\delta}$ [50]. It is assumed that three

cobalt oxidation states (Co^{2+}, Co^{3+}, and Co^{4+}) may all be present simultaneously, but that the iron remains as Fe^{4+} [86]. Using Kröger–Vink notation, "incorporation" and "disproportionation" reactions may be written, respectively, as

$$\frac{1}{2}O_2 + V_O^{\bullet\bullet} + 2Co_{Co}^{\times} \rightleftharpoons O_O^{\times} + 2Co_{Co}^{\bullet}, \tag{96}$$

$$2Co_{Co}^{\times} \rightleftharpoons Co_{Co}^{\prime} + Co_{Co}^{\bullet}. \tag{97}$$

The superscripts "×", "•", and "′" indicate charge relative to the fully occupied crystal lattice, with "×" being neutral, "•" meaning $z_k = +1$, and "′" meaning $z_k = -1$. An oxygen vacancy $V_O^{\bullet\bullet}$ has a $z_k = +2$ charge, relative to the oxygen anion that would ordinarily occupy the site. The reduced cobalt $Co_{Co}^{\prime}$ and oxidized cobalt $Co_{Co}^{\bullet}$ are both expected to behave as small polarons [86].

The equilibrium composition must be constrained by site and charge balances. The charge balance (electroneutrality) is stated as

$$[Co_{Co}^{\bullet}]_L - [Co_{Co}^{\prime}]_L + 2[V_O^{\bullet\bullet}]_L + [Fe_{Co}^{\bullet}]_L - [Sr_{La}^{\prime}]_L = 0. \tag{98}$$

In this expression, the subscript "L" in $[X]_L$ indicates lattice-scale concentrations. In the doped perovskite crystal structure (ABO_3), site balances must be enforced for the A and B sites. The cobalt (B-site) site balance is stated as

$$[Co_{Co}^{\bullet}]_L + [Co_{Co}^{\prime}]_L + [Co_{Co}^{\times}]_L + [Fe_{Co}^{\bullet}]_L = 1. \tag{99}$$

The oxygen site balance requires that

$$[O_O^{\times}]_L + [V_O^{\bullet\bullet}]_L = 3. \tag{100}$$

In this formulation, it is assumed that $[Sr_{La}^{\prime}]_L$ and $[Fe_{Co}^{\bullet}]_L$ are fixed by the doping levels ($La_{1-x}Sr_xCo_{1-y}Fe_yO_{3-\delta}$) as

$$[Sr_{La}^{\prime}]_L = x, \quad [Fe_{Co}^{\bullet}]_L = y. \tag{101}$$

The oxygen non-stoichiometry is assumed to be $\delta = [V_O^{\bullet\bullet}]_L$.

6. Thermal considerations

The design and control of electrochemical devices can be substantially influenced by thermal behaviors. Li-ion battery safety and lifetime, for example, are directly affected by internal heating and thermal runaway. In applications such as fuel cells and electrolyzers, the management of significant heating within the ion-conducting membranes directly affects design and implementation.

The thermal behaviors within electrodes and electrolytes are intimately coupled with the electrochemical processes. Broadly speaking, electrochemical processes produce heat in two ways. *Faradaic* heating is the result of inefficiencies (irreversibilities) in charge-transfer chemistry at the electrode-electrolyte interfaces. *Ohmic* heating (Joule heating) is the result of ionic and electronic fluxes through electrode and electrolyte phases. Additionally, heat release of *thermochemical* (non-charge-transfer) main or side reactions in complex reaction systems contribute to the overall thermal behavior.

6.1. Faradaic heating

The Faradaic heat-generation rate $\dot{q}_{F,i}$ that is associated with a charge-transfer reaction at electrode and electrolyte interfaces can be evaluated as the difference of the enthalpy change and produced electric power from the ith electrochemical reaction. Stated mathematically,

$$\dot{q}_{F,i} = -i_{e,i}\frac{\Delta H_i}{n_{e,i}F} + i_{e,i}\left(\Phi_{ed} - \Phi_{el}\right), \tag{102}$$

where ΔH_i is the enthalpy change associated with the ith charge-transfer reaction.

Considering the general thermodynamic relationships,

$$\Delta H = \Delta G + T\Delta S, \tag{103}$$

with

$$\Delta S = -\left(\frac{\partial(\Delta G)}{\partial T}\right)_p, \tag{104}$$

the enthalpy difference associated with a charge-transfer reaction can be expressed as

$$\begin{aligned}\frac{\Delta H}{n_e F} &= \frac{\Delta G}{n_e F} + T\left[\frac{\partial}{\partial T}\left(-\frac{\Delta G}{n_e F}\right)\right]_p \\ &= E^{eq} - T\left(\frac{\partial E^{eq}}{\partial T}\right)_p.\end{aligned} \tag{105}$$

In this expression, E^{eq} is the equilibrium electrostatic-potential difference across the electrode-electrolyte interface. The equalibrium electrostatic potential E^{eq} is equivalent to the reversal potential E^{REV}.

The heat release associated with charge-transfer

chemistry can be rewritten as

$$\begin{aligned}\dot{q}_{\mathrm{F},i} &= i_{\mathrm{e},i}\left((\Phi_{\mathrm{ed}}-\Phi_{\mathrm{el}})-E_i^{\mathrm{eq}}\right)+i_{\mathrm{e},i}T\left(\frac{\partial E_i^{\mathrm{eq}}}{\partial T}\right)_p \\ &= i_{\mathrm{e},i}\eta_{\mathrm{act},i}+i_{\mathrm{e},i}T\left(\frac{\partial E_i^{\mathrm{eq}}}{\partial T}\right)_p,\end{aligned} \tag{106}$$

which indicates that there are two contributions to the Faradaic heat generation. One is the heat generation due to the inefficiency or activation polarization of the charge-transfer reactions. The other is the reversible entropic heat generation.

6.2. Ohmic heating

Although both electrode and electrolyte materials are conductors, they often offer significant resistances (i.e., relatively low conductivities). Electrodes are usually dominantly electronic conductors and usually have higher conductivities than the electrolytes. The electrolytes are dominantly ion conductors and usually have lower conductivities than the electrolytes. There can be significant Ohmic or Joule heating in both electrodes and electrolytes.

The local ohmic heat production due to ion and electron transport within an electrode or electrolyte can be expressed as

$$\dot{q}_{\mathrm{ohm}} = \frac{\mathbf{i}\cdot\mathbf{i}}{\sigma}, \tag{107}$$

where $\mathbf{i}$ and σ are the current density and conductivity, respectively.

6.3. Heating due to non-charge-transfer reactions

Thermochemical reactions (i.e., reactions without charge transfer) can dominate thermal behavor of electrochemical cells. Examples include the (endothermal) steam reforming in hydrocarbon-fueled SOFCs and the (exothermal) decomposition chemistry taking place in lithium-ion batteries at high temperature, leading to thermal runaway. In a generalized expression, the heat release of an arbitrary reaction is given by

$$\dot{q}_{\mathrm{r},i} = q_i\Big[-\Delta H_i + n_{e,i}F\left(\Phi_{\mathrm{ed}}-\Phi_{\mathrm{el}}\right)\Big], \tag{108}$$

where q_i the reaction rate of progress (cf. Eq. 20). This expression is valid for both electrochemical and thermochemical reactions, as $n_{e,i} = 0$ for the latter. While Eq. 106 shows reversible and irreversible heating as separate terms, the equivalent Eq. 108 is more directly related to the fundamental thermodynamic property ΔH_i and therefore easier to implement in a generalized Marcus formalism.

6.4. Energy balances

The Faradaic and Ohmic heating are ultimately incorporated as terms in energy-conservation equations, with the particular form of the energy equations depending on the geometry being modeled. In all cases, the ohmic heating appears as a source term within a phase-specific conservation equation.

Because the Faradaic heating appears at interfaces between phases, it can participate differently in different models. On one hand, the Faradaic heating could be viewed in the context of a boundary condition for a model that is focused on an electrolyte phase. On the other hand, consider a geometrically complex porous electrode model such as illustrated in Fig. 2. In this case, phase interfaces are distributed throughout the entire domain. If the porous structure is represented as a continuum with phase fractions (e.g., porosity), then the Faradaic heating is usually most easily represented as a source term based on interfacial area per unit volume.

The role of the electrochemistry software is to make functions available that can be used to evaluate the Faradaic and Ohmic heating rates. However, the results of these functions may be used differently in different models of electrochemical systems.

7. Numerical Simulation Concerns

Generally speaking, the modeling tools described herein provide capabilities to calculate thermodynamic properties, electrochemical reaction rates, and transport/flux rates for relevant phases and species. Simulation tools, on the other hand, implement governing equations to describe the spatial and/or temporal evolution of device properties to determine electrochemical device performance. While many simulation software platforms, such as COMSOL, FLUENT, and STAR-CD, are packaged together with embedded modeling tools, the two topics are distinct. The modeling tools provide input values required for solving the governing equations, as described for energy conservation in Section 6.4. In a thermal energy conservation equation, modeling tools provide calculations for terms such as heat generation from chemical or electrochemical reactions or thermal conduction through a flux boundary. The most appropriate modeling tools for a given numerical simulation depends on the simulation requirements (dimensionality, length and time scales, etc.). The appropriate level of complexity for a so-called 'single particle' battery model, for instance, is different from the level best suited for a full 3D simulation on an accurately reconstructed battery microstructure, which in

turn may differ from the modeling approach in a pack-level simulation. Furthermore, the choice of a particular modeling approach may require the use of more sophisticated algorithms and numerics for solving a specific simulation. For example, implementing detailed surface chemistry may require initialization routines to determine internally consistent initial conditions, before integrating a set of governing differential equations.

In this light, the need for (*i*) open, and (*ii*) generalized electrochemical software becomes even more apparent. To correctly match appropriate modeling and simulation approaches, the types of generalized modeling approaches described herein have several potential benefits. First, an *open* software architecture makes the modeling approach transparent, so that appropriate simulation approaches may be identified and/or designed. Thus, associated assumptions with the modeling approach are made explicit to the user. Second, a *generalized* software approach allows the user to efficiently change the level of complexity in the electrochemical physical phenomena with no substantial changes to the simulation routines. For example, switching from the standard intercalation model in Eq. 1 to the two-step mechanism in Eqs. 3 and 2 does not alter the conservation equation for $[X_k]$, the molar density of bulk intercalation species k in the carbon:

$$\frac{\partial [X_k]}{\partial t} = -\nabla \cdot \mathbf{J}_k, \tag{109}$$

where $\mathbf{J}_k$ is the molar flux of species k within the elctrode particle [93, 11]. At the carbon surface, $\mathbf{J}_k$ is equal to the molar production rate due to surface reactions:

$$\mathbf{J}_k|_{r=R} = \dot{s}_k, \tag{110}$$

where $\dot{s}_k$ is the production rate (kmol m^{-2} s^{-1}) of bulk species k due to surface reactions. When written generally in this manner, the modeling software calculates the $\dot{s}_k$ term, according to whichever reactions are specified (either Eq. 1 or Eqs. 3 and 2, in this case). As described in Section 8, the user makes this specification in the input file, with no significant changes to how the underlying governing equations are implemented. Rather, the only change required in this particular example is that governing equations must also be added for θ_k, the coverages of surface species at the carbon-electrolyte interface:

$$\frac{\partial \theta_k}{\partial t} = \frac{n_{\text{surf},k}}{\Gamma_m} \dot{s}_k, \tag{111}$$

where $\dot{s}_k$ is the molar production rate of surface species k due to surface reactions, $n_{\text{surf},k}$ is the number of surface sites occupied by species k, and Γ_m is the total concentration of surface sites (kmol m^{-2}). In this manner, the user can therefore switch easily between levels of electrochemical complexity and readily tune them to adapt for simulations that vary across length, time, and dimensionality scales.

8. Software implementation

As a practical matter, general software implementations are needed. The user should be able to describe the chemistry in terms of clearly written and understandable material properties and reactions, with the software providing the needed functionality to pose and solve complex electrochemistry problems. The challenge for developing such software is much more complex than is the case for homogeneous gas-phase chemistry. At this time, no such *general purpose* electrochemistry is available to assist the research and development of critical electrochemistry applications and technologies.

Broadly speaking, the software must be designed and implemented to fulfill two functions:

- A user interface is needed within which to describe electrochemical kinetics and transport. Meeting this need requires defining a syntax that is sufficiently general to describe relevant complexity, but sufficiently structured so as to make rule-based communication efficient and comfortable. On one hand, if the syntax is too restrictive, then expressing the needed complexity may be impeded. If, on the other hand, the syntax is too general then it effectively becomes a programming language without the practical benefits of a convenient user interface. Finding the appropriate middle ground can be challenging.
- Once the user has communicated the electrochemical kinetics, such as via a reaction mechanism, the software must make functions available that can be accessed by higher-level code to evaluate properties and rates as functions of state variables.

Below, we provide a concrete example of how to implement the required electrochemical functionality within the CANTERA software framework [87]. CANTERA is an open source, object-oriented software library used for calculating thermodynamic, transport, and chemical kinetic properties and rates for user-defined material sets. While the software does include a limited set of simulation tools (mostly applicable to combustion applications), it is primarily a modeling tool. Rather than competing with simulation software such as FLUENT, COMSOL, STAR-CD or others, it can

be coupled to these packages to provide greater flexibilty, transparency, and user input into how thermodynamic, transport, and kinetic terms utilized in the simulations are calculated. This example is written within the CANTERA framework, not as an overt endorsement of that software package over other options, nor as a description of current CANTERA capabilities. In fact, some of the capabilities described below are yet to be implemented. Rather, we use CANTERA for this example because the generalized software *structure* described above is already largely in place within CANTERA, and as such we can provide a sufficiently concrete example of the required user inputs. The primary challenge is to extend the software to embrace increasingly complex electrochemistry.

8.1. User interfaces

As in CHEMKIN and CANTERA, the user initially interacts with a file-based interface to describe a particular electrochemical system and associated thermodynamic, reaction, and transport properties. The general-purpose software makes functions available for use in evaluating terms in conservation equations. The input must specify phases and describe all species within each phase. Input syntax rules must be sufficiently flexible so as to accept any range of commonly available inputs which may be used to specify thermodynamic or transport parameters. For example, species transport properties can be given as either diffusion coefficients or as mobilities. Species activities can be defined by parameters specific to an equation of state, but these parameters can frequently be derived, in part, from fundamental physical parameters such as species critical properties [88].

8.1.1. Phases

Phases play essential roles in electrochemistry, with potentially great differences between the types of phases. For example, liquid-phase electrolytes are very different from solid-phase polycrystalline electrolytes. Many applications involve gas phases (e.g., solid-oxide fuel cells), which have no electrochemically specific attributes within the phase. Similarly, some applications involve heterogeneous reactions that proceed on a catalyst phase.

A phase definition must necessarily identify the physical form of the phase. Then, depending on the phase type, the required attributes can be quite different. For example, in a crystalline phase information is needed about crystal-lattice structure, dopants, etc. Issues such as site-balance and charge-balance constraints are relevant. Liquid phases need no such information, but properties such as phase density and viscosity are required. Additionally, the number of mobile ions or charged defects is very important. Significant simplifications are available for modeling phases with only two mobile ions (i.e., binary systems). Phases with three or more mobile ions require more information and are more complicated to model.

8.1.2. Species and charged defects

Each species or charged defect must be associated with a phase. Moreover, each species requires thermodynamic and transport properties. Thermodynamic properties are usually specified in terms of temperature-dependent fits to heat capacity, enthalpy, and entropy. Unlike the gas phase, the needed properties are often not known. Thus, as new materials and chemistries are developed, an important task is to establish properties for the participating species. This can be a lengthy and difficult task, with the resulting properties often being not entirely unique [67, 68, 36]. As new experimental methods and computational chemistry capabilities are developed to establish these parameters, it is important that general-purpose software can flexibly incorporate input parameters in a variety of forms, such as from atomic-scale *ab initio* simulations.

Transport properties may be represented variously as Onsager coefficients, mobilities, diffusion coefficients, or conductivities, which are generally interconnected. Transport properties for binary systems can benefit from significant simplifications. In addition to binary or multi-component considerations, transport properties may be represented in a dilute limit or may need to be represented using concentrated-solution theories. Of course, more information and material properties are required to represent the concentrated-solution theory. Thus, the user interface must be designed to accommodate different phase identities and the levels of transport theory.

8.1.3. Electrochemical reactions

Electrochemical reactions must be represented in a syntax that is easily understood. Representing electrochemistry in the framework of fundamental Marcus theory is most general. However, any general-purpose software must also be capable of representing charge-transfer reactions in the Butler–Volmer form. The Butler–Volmer approach depends on assumptions and approximations, but is very widely used in the electrochemical literature. As a practical matter, the Marcus and Butler–Volmer representations cannot be easily

mixed within a particular reaction mechanism. Depending on which approach is used, the user may need to provide different information and properties. For example, expressions for reversible potentials are needed in any Butler–Volmer implementation. However, in the Marcus approach accurate thermodynamic properties are required to assure the accurate prediction of reversible potentials and measurable open-circuit voltages.

Another important consideration involves whether or not Kröger–Vink notation is used. With systems involving polycrystalline electrolytes, Kröger–Vink notation is the most natural. However, for systems such as those involving liquid electrolytes, Kröger–Vink notation is usually not appropriate. The Kröger–Vink notation is quite different from the notation commonly used in liquid-phase electrolytes. For example, a proton in a PEM fuel-cell membrane is usually represented as H^+. In the equivalent protonic-ceramic fuel cell with a polycrystalline proton-conducting membrane, the proton is represented as $OH_O^\bullet$, with the leading "O" indicating that the proton is associated with an oxygen site. Additionally, the immobile lattice vacancies are typically modeled as a mobile charged defect in Kröger-Vink notation.

General-purpose electrochemistry software must be capable of using the Kröger–Vink notation, where appropriate, and must be configured to work in a generalized manner with reactions in complex lattice phases that are common in solid-state conductors. Chemical kinetics software (such as CANTERA) verify that user-defined reactions balance elements and charge. In addition, for complex lattice phases the software must also be able to verify that lattice sites are conserved. In other words, a reaction must create or destroy species within the constraints of lattice characteristics. Lattice sites themselves cannot be created or destroyed.

8.2. User Input Example

A user-defined set of inputs in the CANTERA format provides an example of the required structure for a user input file for generalized electrochemical kinetics software calculations. For any generalized software program, the user is required to input information to communicate the following information to the software:

1. *Phase information* –For each phase, the user must specify the following:
   - Phase type
   - Elements involved
   - Species involved
   - Thermodynamic model
   - Transport model

   The thermodynamic model typically consists of an equation of state which provides a framework for calculating both phase-level thermodynamic quantities (e.g. Gibbs energy G and enthalpy H) and $p - v - T$ relationships. Moreover, the thermodynamic and transport models rely on individual species properties, as described below, but any information describing species interactions for either model must be provided at the 'phase' level. Partial molar thermodynamic quantities, for example, are calculated at the 'phase' level.
2. *Species information* – For every species included in a phase declaration, the user must provide:
   - Elements included
   - Species charge
   - Species thermodynamic parameters
   - Species transport parameters

   These parameters pertain to the individual species properties. These are provided to the respective phase's thermodynamic and transport models, which determine how the individual species interact to determine phase and species properties.
3. *Reaction information* – For each reaction, the user must provide the following:
   - Reaction type
   - Reaction equation
   - Reaction rate parameters

Figures 10–12 illustrate examples of how required information is provided to describe lithium intercalation at the interface between a graphite anode phase and a carbonate-based electrolyte. The text from all three figures is entered into a single input file, but are broken out separately here for discussion purposes. This input is framed within the context of a CANTERA input (`CTI`) file. Some of the functionality shown in this example already exists in CANTERA, while other capabilities are yet to be implemented. The model includes binary electrolyte transport to and from the anode-electrolyte interface according to concentrated solution theory, plus a two-step intercalation reaction (Reactions 2 and 3) wherein the lithium first adsorbs/plates on the anode surface (a charge-transfer step), and is subsequently incorporated into the graphite anode (a non-electrochemical interface reaction). More complex chemistry can be incorporated, particularly as related to SEI formation and evolution, but are omitted at present for clarity's sake. Regardless, any additional information will be input in a format similar to that currently shown in the figures.

```
# CTI - Cantera Input file for Lithium intercalation at the interface between
#         a graphite anode and liquid carbonate electrolyte.

#-------------------------------------------------------------------------
#  Phase data
#
#-------------------------------------------------------------------------
# Bulk anode phase:
intercalation_electrode(name = "graphite",
  elements = " C Li E ",
  species = " C6(C_b) LiC6(C_b) electron(C_b) ",
  transport = "dilute_solid",
  thermo = RedlichKister(s1="LiC6(C_b)", s2="C6(C_b)",
    activity_coefficients=(binarySpeciesParameters(
      excess_enthalpy = [-3.268E6, 3.955E6,  -4.573E6, 6.147E6, -3.339E6,
            1.117E7,  2.997E5, -4.866E7,  1.362E5,  1.373E8,
                -2.129E7, -1.722E8,  3.956E7,  9.302E7, -3.280E7],
      excess_entropy = 0.0))),
  molar_density = (3.15e-2, 'mol/cm3'))

# Bulk electrolyte phase:
liquid_electrolyte(name = "electrolyte",
  elements = " C H O Li E F P ",
  species = " Li+(e) PF6-(e) solvent(e) ",
  density = (1.208, 'g/cm3'),
  transport = binary_concentrated_solution(
    cation(name="Li+(e)", stoich=1),
    anion(name="PF6-(e)", stoich=1),
    solvent(name="solvent(e)"),
    viscosity_ref = (0.7, 'cP'),T_ref=293),
  thermo = RedlichKister(s1="Li+(e)", s2="PF6-(e)", s3="solvent(e)",
      activity_coefficients=(multiComponentSpeciesParameters(
        A = [[-1.287E6, 1.723E5,  1.353E6],
             [ 1.417E4, -7.319E7, -3.117E5],
             [-3.216E3,  6.215E5,  1.174E8]]))))

# Anode-electrolyte interface:
ideal_interface(name = "graphite_surf",
   elements = " Li ",
   species = "Li(C_s) (C_s)",
   site_density = (1.07e-5, 'mol/m2'),
   phases = " graphite electrolyte ")
```

Figure 10: Example CANTERA input (CTI) file describing the necessary phase information for intercalation at the interface between a liquid carbonate electrolyte and solid graphite anode. Some of the physical parameters should be considered as illustrative and some of the functionality may not yet be implemented in the released version of CANTERA.

8.3. Phase information

Figure 10 shows the required inputs related to phase information. Three phases are required to describe the intercalation process: a solid electrode phase (named 'graphite,' here), a liquid electrolyte phase ('electrolyte'), and a phase to represent the interface between the two ('graphite_surf').

Graphite electrode – The graphite electrode phase is specified as an 'intercalation_electrode,' which would be linked to a set of governing equations for a solid phase with a lattice-like structure that can host a single intercalating species and which can also conduct electrons. The phase declaration contains lists of the elements and species included in the phase. This particular phase has three species: a C_6 graphite unit cell (a defacto vacancy), LiC_6, a graphite unit cell with intercalated lithium, and a delocalized electron. Each species name includes a reference to its phase ('C_b' = 'Carbon bulk'), thus differentiate it from a similarly-named species in another phase. The graphite phase declaration must also include a 'molar_density' input, which specifies the total molar concentration (kmol m^{-3}) of the available lattices sites. The molar concentration of intercalated lithium sites and vacancies must always sum to the number of available sites. This phase type is unique in that it contains some species bound to lattice sites and an electron which is not. Well defined rules must be established to differentiate the two types of species.

The phase description also specifies transport and thermodynamic models. In this example, transport calculations for species other than electrons use a dilute defect solid model (Section 5.5). Thermodynamic calculations use the Redlich–Kister model [9] to evaluate the excess Gibbs free energy for the intercalation reaction in the following form

$$n_T g^E = [X_{s1}]\,[X_{s2}] \sum_\ell A_\ell \left([X_{s1}] - [X_{s2}]\right)^\ell , \qquad (112)$$

where the bulk lattice only has two species, and A is the vector input for 'excess_enthalpy'. The species are labeled "s1" and "s2" to associate the species with the excess free energies.

Liquid electrolyte – The electrolyte phase declaration proceeds in a manner similar to the electrode phase. It is declared as a 'liquid_electrolyte', which is an incompressible phase, similar to the 'intercalation_electrode', but without any restrictions related to lattice sites and without electrical conductivity. The phase declares three species: a Li^+ cation, a PF_6^- anion, and a solvent. The suffix '(e)' is given to each species name, both for clarity and to differentiate from potential similarly-named species in other phases. A constant mass density is also provided.

The input file instructs the electrolyte transport calculations to use concentrated solution theory for a binary salt in a liquid solvent. At the phase level, the user must indicate which species names correspond to the anion, cation, and solvent, and must specify the stoichiometry of the cation and anion (ν_+ and ν_-, respectively). For the solvent, the user must also provide the viscosity. The phase thermodynamic quantities here will also be calculated using a Redlich–Kister model for the Gibbs excess energy. Because the electrolyte has three interacting species, the 'binarySpeciesParameters' from the graphite electrode cannot be used, here. As described by O'Connell and Haile [46], the binary Redlich–Kister expansion can be extended to a multicomponent form

$$n_T g^E = g_{12} + g_{13} + g_{23}, \qquad (113)$$

$$\frac{g_{ik}}{RT} = [X_i]\,[X_k]\left(A_{ik} + B_{ik}\left([X_i] + [X_k]\right) + \dots\right) \qquad (114)$$

Each term in the expansion requires a series of input matrices of $N_{\text{species}} \times N_{\text{species}}$ species interaction parameters to calculate the excess energy. The example in Fig. 10 is restricted to just a single input matrix A_{ik}.

Anode-electrolyte interface – Finally, the interface between the anode and electrolyte must be defined as a phase. It is specified here as an 'ideal_interface', which dictates the form of the chemical potential calculations. The interface phase must provide lists of elements and species. It must also specify a 'site_density' (i.e., the total number of available sites to host surface species, similar to the 'molar_density' in the graphite phase). Additionally, the interface specification must provide a list of the phases that can participate in any interface reactions. The current mechanism includes an empty surface site (a vacancy, '(C_s)') and an adsorbed lithium species at the graphite–electrolyte interface. However, an interface phase is required even for interfacial reaction mechanisms where no intermediate surface phases are defined (e.g. where the Li ion from the electrolyte is transferred directly to the bulk graphite). This informs the software that the participating bulk phases are in direct physical contact, and to create a separate kinetics manager to calculate relevant terms for reactions involving the participating phases.

8.4. *Species information*

Figure 11 shows an example of the species input format for the phases described in Figure 10. Each species listed in a phase declaration must have its own species declaration in the input file. The species entry must give the species name (which matches that provided in the phase declaration), a chemical formula (which must utilize only those elements listed in the phase declaration), a species thermodynamic entry and a species transport entry. The charge of the species is indicated by the number of electrons in the species (the number of electrons < 0 for a positive charge). Because the Li-ion battery will operate within a relatively narrow temperature range, a relatively simple species thermodynamic model, which assumes a constant specific heat c_p, is specified. Other forms (such as NASA polynomials) are available for incorporating complex temperature dependence. Note also that these terms are used to calculate the ideal, reference-state thermodynamic terms, to which activity and excess energy terms are added, using the information in the phase declaration. Additionally, the thermodynamic entry for the electron species in the carbon bulk specifies a 'metal_electron' model, where the activity is equal to the electrostatic potential times the species charge.

```
#-----------------------------------------------------------------------------
#  Species data
#
#-----------------------------------------------------------------------------
# Anode species:
species( name = "C6(C_b)",
  atoms = " C:6 ",
  thermo = const_cp(h0 = (0.0, 'kcal/mol')),
  transport = intercalation(diffCoeff='None'))

species( name = "LiC6(C_b)",
  atoms = " C:6 Li:1 E:-1",
  thermo = const_cp(h0 = (-11.65, 'kJ/mol'), s0 = (0, 'kJ/mol')),
  transport = intercalation(diffCoeff=(2.0e-16,'m2/s'))

species( name = "electron(C_b)",
  atoms = "E:1",
  thermo = metal_electron,
  transport = metal_electron(conductivity=(1.0e4, 'S/m'))

# Electrolyte species:
species( name = "Li+(e)",
  atoms = " Li:1 E:-1 ",
  thermo = const_cp(h0 = (0.0, 'kJ/mol')),
  transport = Stokes_Einstein(geom='spherical',
          radius = (0.182, 'nm'),
          sliding_factor = 0))

species( name = "PF6-(e)",
  atoms = "P:1, F:6, E:1",
  thermo = const_cp(h0 = (0.0, 'kJ/mol'), s0 = (0.0, 'J/mol/K')),
  transport = Stokes_Einstein(geom='spherical',
          radius = (0.242, 'nm'),
          sliding_factor = 0))

species( name = "Solvent(e)",
  atoms = "C:3, H:4, O:3",
  thermo = const_cp(h0 = (0.0, 'kJ/mol'), s0 = (0.0, 'J/mol/K')),
  transport = 'None')

# Graphite surface species:
species( name = "Li(C_s)",
  atoms = " Li:1 ",
  thermo = const_cp(h0 = (0.0, 'kJ/mol'), s0 = (0.0, 'J/mol/K'),
    cp0 = (3.56, 'kJ/kg/K'), T0 = (298, 'K')),
  transport = 'None')

species( name = "(C_s)",
  atoms = "  ",
  thermo = const_cp(h0 = (0.0, 'kJ/mol'), s0 = (0.0, 'J/mol/K')),
  transport = 'None')
```

Figure 11: Example CANTERA input (CTI) file describing the necessary species information for intercalation at the interface between a liquid carbonate electrolyte and solid graphite anode. Some of the physical parameters should be considered as illustrative and some of the functionality may not yet be implemented in the released version of CANTERA.

The species transport parameters reflect a range of different possible models. The C_6 lattice species ('C6(C_b)'), represents an immobile vacancy. Even though it is immobile, lattice site conservation implies that the vacancy flux must always be equal and opposite to that of the intercalating species. Thus, a transport model ('intercalation') is specified, but no diffusion coefficient is given, indicating the immobile lattice vacancy. In contrast, the 'LiC6(C_s)' species is given the same 'intercalation' transport model, but with a non-zero diffusion coefficient. The electron species in

the graphite is given a 'metal_electron' transport model, where the electronic current density is calculated according to Ohm's law (Eq. 93).

For the cation and anion in the electrolyte, parameters (a geometry label, the ionic radius, and a sliding factor) are provided to evaluate binary diffusion coefficients using the Stokes-Einstein relationship. Again, this is provided simply as an example (cf., Section 5.4). Other more accurate modifications have been developed and can be implemented. Because the solvent self-diffusion coefficient is never explicitly used in the concentrated solution theory outlined in Section 5.3, no species transport information is required. Similarly, because the surface species 'Li(C_s)' and '(C_s)' are considered to be immobile, transport properties are not needed.

8.5. *Reaction information*

Figure 12 shows the necessary reaction inputs to describe the intercalation process. The mechanism includes two steps: Li adsorption/plating onto the graphite surface, which is a charge-transfer reaction, followed by Li incorporation from the surface into the graphite bulk, which is a thermal reaction (i.e. the surface and bulk species involved are all charge-neutral, so the reaction does not transfer any charge between phases). This is slightly more complex than the one-step mechanism in Reaction 1, but additional chemical complexity would certainly be required to incorporate processes such as Li plating and dendrite growth or SEI formation and evolution.

Each reaction entry requires, at minimum, a reaction equation string and inputs to evaluate reaction rate parameters. For the charge-transfer reaction, the rate parameters are given in a Butler-Volmer formulation, which includes Arrhenius parameters for the exchange current density prefactor k_{ct} and the forward symmetry factor β_f. The three Arrhenius parameters for k_{ct} correspond to $[A_i, n_i, E_i]$ respectively (see Eq. 25). Omitting the backward symmetry factor β_b triggers the default assumption that $\beta_f + \beta_b = 1$. Furthermore, while the foregoing equations (e.g. Sec. 4.1) were written using β_a and β_c and assuming the reaction is written such that the forward reaction is anodic in nature, for generalized software no such assumptions should be made, allowing for greater user flexibility. For the incorporation reaction, Arrhenius parameters are given for the thermally activated rate coefficient $k_{\mathrm{f}}^{\mathrm{t}}$ (Eq. 25).

```
#-------------------------------------------------------------------------------
# Reaction data
#-------------------------------------------------------------------------------
# Surface reaction 1: charge transfer of Li+(e) to Li(C_s):
surface_reaction("Li+(e) + electron(C_b) + (C_s) <=> Li(C_s)",
exchangecurrentdensity([4.3611, 0.0, 0.0],beta_f=0.5))
# Surface reaction 2: Li(C_s) incorporation into graphite:
surface_reaction("Li(C_s) + C6(C_b) <=> (C_s) + LiC6(C_b)",
Arrhenius([2.3e3, 0.0, 0.0]))
```

Figure 12: Example CANTERA input (CTI) file describing the necessary reaction information for intercalation at the interface between a liquid carbonate electrolyte and solid graphite anode. Some of the physical parameters should be considered as illustrative and some of the functionality may not yet be implemented in the released version of CANTERA.

9. Summary and conclusions

Although numerous important technologies depend on electrochemistry, to date there are no general-purpose modeling tools available to handle complexity in electrochemical transport and kinetics. The present paper seeks to articulate a vision about the scientific needs for modeling electrochemical processes. In fact, the underpinning theories are well known and generally well documented. However, the software implementations have not been fully developed and documented.

The general approach follows the lead of CHEMKIN and CANTERA software. That is, enable the user to define an electrochemical system using a convenient file-format syntax. In this context, "define" means to specify the characteristics of phases, interfaces between phases, species that exist within phases, and reactions that proceed within phases and a phase interfaces. The specifications involve thermodynamic and transport properties as well as rate expressions.

Building on the foundation of current capabilities, current software should be extended to incorporate increasingly complex aspects of electrochemical kinetics and transport. CANTERA provides one example of a generalized modeling framework that already has some significant electrochemical capabilities. However, because electrochemistry is inherently complicated, compared, for example, to gas-phase chemistry, developing and validating the needed capabilities for any software package is a substantial undertaking.

The software discussed in this paper can play a major beneficial role in the development of a wide range of new electrochemical technologies. Advanced predictive modeling capabilities can substantially impact the interpretation of experimental findings and improve scientific understanding. Such capabilities also assist to improve and accelerate the pace of technology development.

Acknowledgments

This research was supported by the Air Force Office of Scientific Research via grant FA9550-16-1-0349 and by the Office of Naval Research via grant N00014-16-1-2780. This work was authored in part by the National Renewable Energy Laboratory, operated by Alliance for Sustainable Energy, LLC, for the U.S. Department of Energy (DOE) under Contract No. DE-AC36-08GO28308. Funding provided by the U.S. DOE Office of Vehicle Technology Energy Storage Program, program manager Brian Cunningham. The views expressed in the article do not necessarily represent the views of the DOE or the U.S. Government. The U.S. Government retains and the publisher, by accepting the article for publication, acknowledges that the U.S. Government retains a nonexclusive, paid-up, irrevocable, worldwide license to publish or reproduce the published form of this work, or allow others to do so, for U.S. Government purposes.

[1] K. Kang, Y. Meng, J. Bréger, C. Grey, G. Ceder, Electrodes with high power and high capacity for rechargeable lithium batteries, Science 311 (2006) 977–980.

[2] B. Kang, G. Ceder, Battery materials for ultrafast charging and discharging, Nature 458 (2009) 190–193.

[3] D. Aurbach, B. Markovsky, I. Weissman, E. Levi, Y. Ein-Eli, On the correlation between surface chemistry and performance of graphite negative electrodes for Li-ion batteries, Electrochim. Acta 45 (1999) 67–86.

[4] S.-W. Kim, D.-H. Seo, X. Ma, G. Ceder, K. Kang, Electrode materials for rechargeable sodium-ion batteries: Potential alternatives to current lithium-ion batteries, Adv. Energy Mats. 2 (2012) 710–721.

[5] A. Jain, S. Ong, G. Hautier, W. Chen, W. Richards, S. Dacek, S. Cholia, D. Gunter, D. Skinner., G. Ceder, K. Persson, Commentary: The materials project: A materials genome approach to accelerating materials innovation, Apl. Mater. 1, 011002 (2013).

[6] V. Srinivasan, J. Newman, Discharge model for lithium iron-phosphate electrode, J. Electrochem. Soc. 151 (2004) A1517–A1529.

[7] T. Fuller, M. Doyle, J. Newman, Simulation and optimization of the dual lithium insertion cell, J. Electrochem. Soc. 141 (1994) 1–9.

[8] M. Guo, G. Sikha, R. White, Single-particle model for a lithium-ion cell: Thermal behavior, J. Electrochem. Soc. 158 (2011) A122–A132.

[9] A. Colclasure, R. Kee, Thermodynamically consistent modeling of elementary electrochemistry in lithium-ion batteries, Electrochim. Acta 55 (2010) 8960–8973.

[10] J. Christensen, J. Newman, A mathematical model for the lithium-ion negative electrode solid electrolyte interphase, J. Electrochem. Soc. 151 (2004) A1977–A1988.

[11] A. Colclasure, K. Smith, R. Kee, Modeling detailed chemistry and transport for solid-electrolyte-interface (SEI) films in Li-ion batteries, Electrochim. Acta 58 (2011) 33–43.

[12] J. Newman, K. Thomas-Alyea, Electrochemical Systems, 3rd Edition, John Wiley & Sons Inc., Hoboken, New Jersey, 2004.

[13] A. Bard, L. Faulkner, Electrochemical Methods Fundamentals and Applications, Wiley, Hoboken, NJ, 2001.

[14] J. Bockris, A. Reddy, M. Gamboa-Aldeco, Modern electrochemistry: Fundamentals of electrodics, 2nd Edition, Kluver Academic/Plenum Publishers, New York, 2000.

[15] T. Fuller, J. Harb, Electrochemical engineering, Wiley, Hoboken, NJ, 2018.

[16] M. Doyle, T. Fuller, J. Newman, Modeling of galvanostatic charge and discharge of the lithium/polymer/insertion cell, J. Electrochem. Soc. 140 (1993) 1526–1533.

[17] M. Doyle, T. Fuller, J. Newman, Relaxation phenomena in lithium-ion-insertion cells, J. Electrochem. Soc. 141 (1994) 982–990.

[18] F. Hall, S. Wußler, H. Buqa, W. Bessler, Asymmetry of discharge/charge curves of lithium-ion battery intercalation electrodes, J. Phys. Chem. C 120 (41) (2016) 23407–23414.

[19] A. Wiedemann, G. Goldin, S. Barnett, H. Zhu, R. Kee, Effects of three-dimensional cathode microstructure on the performance of lithium-ion battery cathodes, Electrochim. Acta 88 (2013) 1580–1588.

[20] M. Farkhondeh, M. Safari, M. Pritzker, M. Fowler, T. Han, J. Wang, C. Delacourt, Full-range simulation of a commercial $LiFePO_4$ electrode accounting for bulk and surface effects: A comparative analysis, J. Electrochem. Soc. 161 (2014) A201–A212.

[21] M. Farkhondeh, M. Pritzker, M. Fowler, C. Delacourt, Mesoscopic modeling of a $LiFePO_4$ electrode: Experimental validation under continuous and intermittent operating conditions, J. Electrochem. Soc. 164 (2017) E3040–E3053.

[22] B. Orvananos, T. Ferguson, H.-C. Yu, M. Bazant, K. Thornton, Particle-level modeling of the charge-discharge behavior of nanoparticulate phase-spearating Li-ion battery electrodes, J. Electrochem. Soc. 161 (2014) A535–A546.

[23] W. Dreyer, J. Jamnik, C. Guhlke, R. Huth, J. Moškon, M. Gaberšček, The thermodynamic origin of hysteresis in insertion batteries, Nat. Mater. 9 (2010) 448–453.

[24] R. Malik, A. Abdellahi, G. Ceder, A critical review of the Li insertion mechanisms in $LiFePO_4$ electrodes, J. Electrochem. Soc. 160 (2013) A3179–A3197.

[25] H. Zhu, R. Kee, Computational modeling of sodium-iodine secondary batteries, Electrochim. Acta 219 (2016) 70–81.

[26] M. Armand, J.-M. Tarascon, Building better batteries, Nature 451 (2008) 652–657.

[27] D. Grübl, B. Bergner, D. Schröder, J. Janek, W. Bessler, Multi-step reaction mechanisms in nonaqueous lithium–oxygen batteries with redox mediator: A model-based study, J. Phys. Chem. C 120 (43) (2016) 24623–24636.

[28] J. Neidhardt, D. Fronczek, T. Jahnke, T. Danner, B. Horstmann, W. Bessler, A flexible framework for modeling multiple solid, liquid and gaseous phases in batteries and fuel cells, J. Electrochem. Soc. 159 (2012) A1528–A1542.

[29] B. Horstmann, T. Danner, W. Bessler, Precipitation in aqueous lithium–oxygen batteries: A model-based analysis, Energy Environ. Sci. 6 (4) (2013) 1299.

[30] Y. Yin, C. Gaya, A. Torayev, V. Thangavel, A. Franco, Impact of Li_2O_2 particle size on Li-O_2 battery charge process: Insights from a multiscale modeling perspective, J. Phys. Chem. Lett. 7 (19) (2016) 3897–3902.

[31] A. Hofmann, D. Fronczek, W. Bessler, Mechanistic modeling of polysulfide shuttle and capacity loss in lithium–sulfur batteries, J. Power Sources 259 (2014) 300–310.

[32] H. Zhu, R. Kee, Modeling protonic-ceramic fuel cells with porous composite electrodes in a button-cell configuration, J. Electrochem. Soc. 164 (2017) F1400–F1411.

[33] H. Zhu, R. Kee, V. Janardhanan, O. Deutschmann, D. Goodwin, Modeling elementary heterogeneous chemistry and electrochemistry in solid-oxide fuel cells, J. Electrochem. Soc. 152 (2005) A2427–A2440.

[34] D. Goodwin, H. Zhu, A. Colclasure, R. Kee, Modeling electrochemical oxidation of hydrogen on Ni-YSZ pattern anodes, J. Electrochem. Soc. 156 (2009) B1004–B1021.

[35] C. Duan, J. Tong, M. Shang, S. Nikodemski, M. Sanders, S. Ricote, A. Almansoori, R. O'Hayre, Readily processed protonic

ceramic fuel cells with high performance at low temperature, Science 349 (2015) 1321–1326.
[36] H. Zhu, S. Ricote, W. Coors, R. Kee, Interpreting equilibrium-conductivity and conductivity-relaxation measurements to establish thermodynamic and transport properties for multiple charged defect conducting ceramics, Farad. Discuss. 182 (2015) 49–74.
[37] M. Shang, J. Tong, R. O'Hayre, A promising cathode for intermediate temperature protonic ceramic fuel cells: $BaCo_{0.4}Fe_{0.4}Zr_{0.2}O_{3-\delta}$, RSC Adv. 3 (36) (2013) 15769–15775.
[38] C. Duan, J. Tong, M. Shang, S. Nikodemski, M. Sanders, S. Ricote, A. Almansoori, R. O'Hayre, Readily processed protonic ceramic fuel cells with high performance at low temperatures, Science 349 (6254) (2015) 1321–1326.
[39] C. Duan, D. Hook, Y. Chen, J. Tong, R. O'Hayre, Zr and Y co-doped perovskite as a stable, high performance cathode for solid oxide fuel cells operating below 500°C, Energy Environ. Sci. 10 (1) (2017) 176–182.
[40] C. Duan, R. Kee, H. Zhu, C. Karakaya, Y. Chen, S. Ricote, A. Jarry, E. Crumlin, D. Hook, R. Braun, N. Sullivan, R. O'Hayre, Highly durable, coking and sulfur tolerant, fuel-flexible protonic ceramic fuel cells, Nature 557 (7704) (2018) 217–222.
[41] H. Malerød-Fjeld, D. Clark, I. Yuste-Tirados, R. Zanón, D. Catalán-Martinez, D. Beeaff, S. Morejudo, P. Vestre, T. Norby, R. Haugsrud, J. Serra, C. Kjølseth, Thermo-electrochemical production of compressed hydrogen from methane with near-zero energy loss, Nat. Energy 2 (2017) 923–931.
[42] C. Karakaya, R. Kee, Progress in the direct catalytic conversion of methane to fuels and chemicals, Prog. Energy Combust. Sci. 55 (2016) 60–97.
[43] R. Kee, C. Karakaya, H. Zhu, Process intensification in the catalytic conversion of natural gas to fuels and chemicals, Proc. Combust. Inst. 36 (2017) 51–76.
[44] S. Morejudo, R. Zanón, S. Escolástico, I. Yuste-Tirados, H. Malerød-Fjeld, P. Vestre, W. Coors, A. Martínez, T. Norby, J. Serra, C. Kjølseth, Direct conversion of methane to aromatics in a catalytic co-ionic membrane reactor, Science 353 (2016) 563–566.
[45] C. Karakaya, S. Hernández-Morejudo, H. Zhu, R. Kee, Catalytic chemistry for methane dehydroaromatization (MDA) on a bifunctional Mo/HZSM-5 catalyst in a packed bed, Ind. Eng. Chem. Res. 55 (2016) 9895–9906.
[46] J. O'Connell, J. M. Haile, Thermodynamics: Fundamentals for applications, Cambridge University Press, Cambridge, NY, 2005.
[47] S. Bishop, D. Marrocchelli, C. Chatzichristodoulou, N. Perry, M. Mogensen, H. Tuller, E. Wachsman, Chemical expansion: Implications for electrochemical energy storage and conversion devices, Annu. Rev. Mater. Res. 44 (2014) 205–239.
[48] T. Ferguson, M. Bazant, Nonequilibrium thermodynamics of porous electrodes, J. Electrochem. Soc. 159 (2012) A1967–A1985.
[49] V. Malavé, J. R. Berger, P. A. Martin, Concentration-dependent chemical expansion in lithium-ion battery cathode particles, J. Appl. Mech. 81 (2014) 091005.
[50] B. Euser, J. Berger, H. Zhu, R. Kee, Defect-transport-induced stress in mixed ionic-electronic conducting (MIEC) ceramic membranes, J. Electrochem. Soc. 163 (2016) F264–F271.
[51] D. Marrocchelli, N. Perry, S. Bishop, Understanding chemical expansion in perovskite-structured oxides, Phys. Chem. Chem. Phys. 17 (2015) 10028–10039.
[52] S. Adler, Chemical expansivity of electrochemical ceramics, J. Am. Ceram. Soc. 84 (2001) 2117–2119.
[53] J. Li, Physical chemistry of some microstructural phenomena, Metall. Trans. A 9A (1978) 1350–1380.
[54] F. Yang, Interaction between diffusion and chemical stresses, Mater. Sci. Eng. A. 409 (2005) 153–159.
[55] H. Zhu, R. Kee, Modeling distributed charge-transfer processes in SOFC membrane electrode assemblies, J. Electrochem. Soc. 155 (2008) B715–B729.
[56] W. Bessler, J. Warnatz, D. Goodwin, The influence of equilibrium potential on the hydrogen oxidation kinetics of SOFC anodes, Solid State Ion. 177 (2007) 3371–3383.
[57] R. Kee, M. Coltrin, P. Glarborg, H. Zhu, Chemically reacting flow: Theory, modeling and simulation, 2nd Edition, Wiley, Hoboken, NJ, 2018.
[58] M. Bazant, Theory of chemical kinetics and charge transfer based on nonequalibrium thermodynamics, Acc. Chem. Res. 46 (2012) 1144–1160.
[59] C. Kupper, W. Bessler, Multi-scale thermo-electrochemical modeling of performance and aging of a $LiFePO_4$/graphite lithium-ion cell, J. Electrochem. Soc. 164 (2) (2017) A304–A320.
[60] J. Owejan, J. Owejan, S. DeCaluwe, J. Dura, Solid electrolyte interphase in Li-ion batteries: Evolving structures measured in situ by neutron reflectometry, Chem. Mater. 24 (11) (2012) 2133–2140.
[61] A. Cresce, S. Russell, D. Baker, K. Gaskell, K. Xu, In situ and quantitative characterization of solid electrolyte interphases, Nano Lett. 14 (3) (2014) 1405–1412.
[62] H. Zhu, R. Kee, Membrane polarization in mixed-conducting ceramic fuel cells and electrolyzers, Int. J. Hydrogen Energy 41 (2016) 2931–2943.
[63] M. Safari, M. Morcrette, A. Teyssot, C. Delacourt, Multimodal physics-based aging model for life prediction of Li-ion batteries, J. Electrochem. Soc. 156 (3) (2009) A145–A153.
[64] S. Vilekar, R. Datta, The effect of hydrogen crossover on open-circuit voltage in polymer electrolyte membrane fuel cells, J. Power Sources 195 (8) (2010) 2241–2247.
[65] M. Bazant, K. Thornton, A. Ajdari, Diffuse-charge dynamics in electrochemical systems, Phys. Rev. E 70 (2004) 021506.
[66] E. Vøllestad, H. Zhu, R. Kee, Interpretation of defect and gas-phase fluxes through mixed-conducting ceramics using Nernst–Planck–Poisson and integral formulations, J. Electrochem. Soc. 161 (2014) F114–F124.
[67] S. Ricote, H. Zhu, W. Coors, C. Chatzichristodoulou, R. Kee, Equilibrium and transient conductivity for gadolium-doped ceria under large perturbations: I. Experiments, Solid State Ion. 265 (2014) 22–28.
[68] H. Zhu, S. Ricote, W. Coors, C. Chatzichristodoulou, R. Kee, Equilibrium and transient conductivity for gadolium-doped ceria under large perturbations: II. Modeling, Solid State Ion. 268 (2014) 198–207.
[69] R. Bird, W. Steward, E. Lightfoot, Transport phenomena, John Wiley & Sons, 1960.
[70] L. Onsager, Theories and problems of liquid diffusion, Ann. N.Y. Acad. Sci. 46 (1945) 241–265.
[71] R. Pollard, J. Newman, Transport equations for a mixture of two binary molten salts in a porous electrode, J. Electrochem. Soc. 126 (1979) 1713–1717.
[72] J. Newman, D. Bennion, C. Tobias, Mass transfer in concentrated binary electrolytes, Ber. Bunsenges. Phys. Chem. 69 (1965) 608–612.
[73] H. Tyrrell, K. Harris, Diffusion in liquids: A theoretical and experimental study, Butterworth & Co, Oxford, UK, 1984.
[74] L. Onsager, R. Fuoss, Irreversible processes in electrolytes. Diffusion, conductance, and viscous flow in arbitrary mixtures of strong electrolytes, J. Phys. Chem. 36 (1932) 2689–2778.
[75] L. Belfiore, Transport phenomenal for chemical reactor design, John Wiley & Sons, Hoboken, New Jersey, 2003.
[76] J. Happel, H. Brenner, Low Reynolds number hydrodynamics: with special application to particulate media, Prentice-Hall, Upper Saddle River, NJ, 1965.
[77] B. Poling, J. Prausnitz, J. O'Connell, The properties of gases and

liquids, McGraw-Hill, 1977.
[78] J.-F. Dufrêche, O. Bernard, S. Durand-Vidal, P. Turq, Analytical theories of transport in concentrated solutions from the MSA, J. Phys. Chem. B 109 (2005) 9873–9884.
[79] N. Shaffer, S. Baalrud, J. Daligault, Effective potential theory for diffusion in binary ionic mixtures, Phys. Rev. E 95 (2017) 013206.
[80] T. Thacher, J.-L. Lin, C. Mou, Theory of Onsager phenomenological coefficients for isothermal linear transport processes in electrolyte solutions, J. Chem. Phys. 81 (1984) 2053–2063.
[81] E. Lai, F. Ciucci, Mathematical modeling of porous batter electrodes – Revisit of Newman's model, Electrochim. Acta 56 (2011) 4369–4377.
[82] S. Hein, A. Latz, Influence of local lithium metal deposition in 3D microstructures on local and global behavior of Lithium-ion batteries, Electrochim. Acta 201 (2016) 354–365.
[83] H.-I. Yoo, M. Martin, J. Janek, Comment on "How to interpret Onsager cross terms in mixed ionic electronic conductors" by I. Riess, Phys. Chem. Chem. Phys. 17 (2015) 11103–111106.
[84] D.-K. Lee, H.-I. Yoo, Electron-ion interface and Onsager reciprocity in mixed ionic-electronic transport in TiO_2, Phys. Rev. Lett. 97 (2006) 255901.
[85] C. Chatzichristodoulou, W.-S. Park, H.-S. Kim, P. Hendriksen, H.-I. Yoo, Experimental determination of the Onsager coefficients of transport for $Ce_{0.8}Pr_{0.2}O_{2-\delta}$, Phys. Chem. Chem. Phys. 12 (2010) 9637–9649.
[86] A. Zuev, V. Sereda, D. Tsvetkov, Defect structure and defect-induced expansion of doped perovskite $La_{0.7}Sr_{0.3}Co_{0.9}Fe_{0.1}O_{3-\delta}$, Int. J. Hydrog. Energy 39 (2014) 21553–21560.
[87] D. G. Goodwin, H. K. Moffat, R. L. Speth, Cantera: An object-oriented software toolkit for chemical kinetics, thermodynamics, and transport processes, http://www.cantera.org, version 2.3.0 (2017).
[88] G. Kogekar, C. Karakaya, G. Liskovich, M. Oehlschlaeger, S. DeCaluwe, R. Kee, Impact of non-ideal behavior on ignition delay and chemical kinetics in high-pressure shock tube reactors, Comb. Flame 189 (2018) 1–11.
[89] R.E. Jones, D.K. Ward, F.S. Gittleson, M.E. Foster, Assessing Electrolyte Transport Properties with Molecular Dynamics, J. Electrochem. Soc. 164 (2017) A1258–1267.
[90] R.E. Jones, D.K. Ward, F.S. Gittleson, M.E. Foster, Assessing electrolyte transport properties with molecular dynamics, J. Electrochem. Soc. 164 (2017) A1258–1267.
[91] T.S. Thatcher, J Lin, C.Y. Mou, Theory of Onsager phenomenological coefficients for isothermal linear transport processes in electrolyte solutions, J. Chem. Phys. 81 (1984) 2053–2063.
[92] A.M. Bizeray, D.A. Howey, C.W. Monroe, Resolving a discrepancy in diffusion potentials, with a case study for Li-ion batteries, J. Electrochem. Soc. 163 (2016) E223–E229.
[93] K.E. Thomas, J. Newman, R.M. Darline, Mathematical Modeling of Lithium Batteries,In W.A. van Schalkwijk, B. Scrosati, editor, *Advances in Lithium-Ion Batteries*, ch. 12,345–392, Kluwer Academic Publishers, New York.

Nomenclature

Variable	Description
a_k	Activity concentrations of species k [kmol, m]
A_i	Pre-exponential factor of reaction i [kmol, m, s]
A_ℓ	Prefactor for excess Gibbs energy [kmol, m, s]
A_{ik}, B_{ik}	Matrix inputs for Redlich–Kister expression [kmol, m]
c_p	Specific heat [J kg^{-1} K^{-1}]
C	Concentration of binary salt [kmol m^{-3}]
D	Diffusion coeff. in binary concentrated solutions [m^2 s^{-1}]
D_k	Diffusion coeff. of species k [m^2 s^{-1}]
$D_{k,\mathrm{eff}}$	Effective diffusion coeff. of species k [m^2 s^{-1}]
$\mathcal{D}$	Ambipolar diffusion coeff. [m^2 s^{-1}]
$\mathcal{D}_{kj}$	Binary diffusion coeff. [m^2 s^{-1}]
E	Young's modulus [N m^{-2}]
E_a	Electric-potential difference between an and el [V]
E_a^eq	Equilibrium potential difference between an and el [V]
E_c	Electric-potential difference between ca and el [V]
E_c^eq	Equilibrium potential difference between ca and el [V]
E^eq	Equilibrium potential difference between ed and el [V]
E_i^eq	Equilibrium potential difference between ed and el for reaction i [V]
E_i	Activation energy of reaction i [J kmol^{-1}]
E^OCV	Open-circuit potential [V]
E_i^REV	Reversible potential of reaction i [V]
F	Faraday constant [s A kmol^{-1}]
g^E	Excess Gibbs free energy due to mixing [J kmol^{-1}]
g_{ik}	Gibbs energy for mixture of species i and k [J]
G	Gibbs free energy [J]
ΔG_i°	Change in standard-state Gibbs free energy [J kmol^{-1}]
ΔH_i	Change in enthalpy for reaction i [J]
$\mathbf{i}$	Current density [A m^{-2}]
i_0	Exchange current density [A m^{-2}]
i_0^*	Exchange current density prefactor [A m kmol^{-1}]
i_e	Butler–Volmer current density [A m^{-2}]
$\mathbf{J}_k$	Flux of species k [kmol m^{-2} s^{-1}]
k_B	Boltzmann constant [J K^{-1}]
k_bi	Backward rate constant for reaction i [kmol, m, s]
k_bi^t	Thermal backward rate constant for reaction i [kmol, m, s]
k_ct	Charge transfer rate coefficient [kmol, m, s]
k_{fi}	Forward rate constant for reaction i [kmol, m, s]
k_{fi}^t	Thermal forward rate constant for reaction i [kmol, m, s]
K_i	Reaction equilibrium constant for reaction i [kmol, m, s]
K_{kj}	Friction coeff. matrix [J s m^{-5}]
L_{kj}	Onsager coeff. matrix [kmol^2 J^{-1} m^{-1} s^{-1}]
L_{kj}^0	Negative inverted matrix of M_{kj}^0 [m^5 s^{-1} J^{-1}]
m	Molality and phase index [mol kg^{-1}, -]
M_{kj}	Modified friction coefficient matrix [J s m^{-5}]
M_{kj}^0	Modified M_{kj} matrix [J s m^{-5}]
$n_\mathrm{e,i}$	Electrons transfered in reaction i [-]
n_i	Temperature exponent [-]
n_k	Kilomoles of species k [kmol]
$n_{\mathrm{surf},k}$	Number of surface sites occupied by species k [-]
n_T	Total kilomoles in solution [kmol]
N_species	Number of species in solution [-]
p	Pressure [Pa]
p_i^*	Inverse equilibrium constants for reaction i [kmol, m, s]
p_k	Partial pressure of species k [Pa]
q_{bi}	Backward rate of progress for reaction i [kmol, m, s]
q_{fi}	Forward rate of progress for reaction i [kmol, m, s]
$\dot{q}_{\mathrm{F},i}$	Faradaic heat generation rate for reaction i [W m^{-2}]
q_i	Rate of progress for reaction i [kmol, m, s]
$\dot{q}_\mathrm{ohm}$	Ohmic heat generation rate [W m^{-3}]
r_k	Radius of species k [m]
R	Universal gas constant [J kmol^{-1} K^{-1}]
$\dot{s}_k$	Molar production rate of surface species k [kmol m^{-2} s^{-1}]
S	Entropy [J K^{-1}]
t	Time [s]
t_k	Transference number of species k [-]
t_k^0	Transference number of species k based on species 0 [-]
T	Temperature [K]
u_k	Mobility of species k [kmol m^2 J^{-1} s^{-1}]
$\mathbf{v}$	Bulk velocity [m s^{-1}]
$\mathbf{v}_k$	Diffusive velocity of species k [m s^{-1}]
W_k	Molecular weight of species k [kg kmol^{-1}]
x, y	Intercalation fraction [-]
X_k	Mole fraction of species k [-]
$[X_k]$	Concentration of species k [kmol m^3]
$\left[X_k^\circ\right]$	Standard state concentration of species k [kmol m^3]
Y_k	Mass fraction of species k [-]
z_k	Charge of species k [-]
α_a	Anodic transfer coeff. [-]
α_c	Cathodic transfer coeff. [-]
β	Symmetry factor [-]
β_a	Anodic symmetry factor [-]
β_{ai}	Anodic symmetry factor for reaction i [-]
β_c	Cathodic symmetry factor [-]
β_{ci}	Backward symmetry factor for reaction i [-]
β_f	Forward symmetry factor [-]
ϵ	Phase dielectric constant [F m^{-1}]
ϵ_m	Volume fraction for phase m [-]

ζ	Friction coeff. [kg s^{-1}]
γ_k	Activity coeff. of species k [-]
$\gamma_\pm$	Binary concentrated solution mean molal activity coeff. [mol kg^{-1}]
Γ_m	Total available surface site density of phase m [kmol m^{-2}]
η_{act}	Activation overpotential [V]
η_j	Viscosity of solvent j [Pa s]
$\theta_{k,m}$	Site fraction of species k on surface of phase m [-]
μ_k	Chemical potential of species k [J $kmol^{-1}$]
μ_k°	Standard-state chemical potential of species k [J $kmol^{-1}$]
$\tilde{\mu}_k$	Electrochemical potential of species k [J $kmol^{-1}$]
ν	Poisson's ratio [-]
ν_+	Cation stoichiometric coefficient in binary mixture [-]
ν_-	Anion stoichiometric coefficient in binary mixture [-]
ν'_{ki}	Forward stoichiometric coeff. for kth species in ith reaction [-]
ν''_{ki}	Reverse stoichiometric coeff. for kth species in ith reaction [-]
ν_{ki}	Net stoichiometric coeff. for kth species in ith reaction [-]
ρ	Local charge density [C m^{-3}]
ρ_m	Density of phase m [kg m^{-3}]
σ	Ionic/electric conductivity [Ω^{-1} m^{-1}]
σ_{h}	Hydrostatic stress [N m^{-2}]
σ_{eff}	Effective conductivity [Ω^{-1} m^{-1}]
υ	Sliding coeff. [-]
Φ_k	Electrostatic potential of species k [V]
Φ_m	Electrostatic potential of phase m [V]
χ_k	Chemical symbol for the species k [-]
$\dot{\omega}_k$	Volumetric production rate of species k [kmol m^{-3} s^{-1}]
Ω_k	Partial molar volume of species k [m^3 kmol]